TWIST1 expression is associated with high-risk Neuroblastoma and promotes Primary and Metastatic Tumor Growth

Maria-Vittoria Sepporta[1], Viviane Praz[1,2], Katia Balmas Bourloud[1], Jean-Marc Joseph[3], Nicolas Jauquier[3], Nicolo' Riggi[2], Katya Nardou-Auderset[1,4], Audrey Petit[5,6], Jean-Yves Scoazec[7], Hervé Sartelet[5,8], Raffaele Renella[1], Annick Mühlethaler-Mottet[1*]

[1]Pediatric Hematology-Oncology Research Laboratory, Woman-Mother-Child Department, Lausanne University Hospital and University of Lausanne, Switzerland;

[2]Experimental Pathology, Lausanne University Hospital and University of Lausanne, Switzerland;

[3]Pediatric Surgery, Woman-Mother-Child Department, Lausanne University Hospital and University of Lausanne, Switzerland.

[4]Ophthalmic Hospital Jules-Gonin - Fondation Asile Des Aveugles, Lausanne, Switzerland

[5]Department of Pathology, Medical University of Grenoble, Grenoble, France

[6]Pediatric Hematology Oncology Department, CHU de la Timone, Marseille, France

[7]Department of Biology and Medical Pathology, Gustave Roussy Institute, Villejuif, France

[8]Department of Biopathology, CHRU de Nancy, Université de Lorraine, Nancy, France

*Contact information: Annick.Muhlethaler@chuv.ch

Keywords: Neuroblastoma, TWIST1/2, Metastasis, Extracellular Matrix, Myofibroblasts, Tumor Microenvironment, Tumor-Stroma Crosstalk

Abstract

The embryonic transcription factors TWIST1/2 are frequently overexpressed in cancer, acting as multifunctional oncogenes. Here we investigate their role in neuroblastoma (NB), a heterogeneous childhood malignancy ranging from spontaneous regression to dismal outcomes despite multimodal therapy. We first reveal the association of TWIST1 expression with poor survival and metastasis in primary NB, while TWIST2 correlates with good prognosis. Secondly, suppression of TWIST1 by CRISPR/Cas9 results in a reduction of tumor growth and metastasis in immunocompromised mice. Moreover, TWIST1 knockout tumors display a less aggressive cellular morphology and a reduced disruption of the extracellular matrix (ECM) reticulin network. Additionally, we identify a TWIST1-mediated transcriptional program associated with dismal outcome in NB and involved in the control of pathways mainly linked to the signaling, migration, adhesion, the organization of the ECM, and the tumor cells versus tumor stroma crosstalk. Taken together, our findings suggest TWIST1 as novel therapeutic target in NB.

Introduction

Neuroblastoma (NB) is the most prevalent solid extra cranial tumor of childhood[1]. While it accounts for approximately 5% of all pediatric cancer, it contributes for 12% of all pediatric deaths[2,3]. Primary tumors can arise along the sympathetic chains and in the adrenal medulla[1,4]. NB is both biologically and clinically heterogeneous. It spans from tumors with favorable biology that can spontaneously regress, to high-risk disease frequently relapsing or refractory to multimodal treatments and responsible for 50-60% of mortality[1,4]. Prognosis is associated with a number of factors, including International Neuroblastoma Risk Group (INRG) stages, age at diagnosis, histopathological classification, the presence of segmental chromosomal alterations[1,5], the activation of telomere maintenance mechanisms[6,7] and somatic mutations in the RAS/MAPK and p53 pathway[7]. Amplification of the proto-oncogene MYCN (MNA) is present in more than 20% of primary NB and in 40-50% of patients with high-risk (HR) disease. It is the most important biological predictor of a poor clinical response[2].

As for most pediatric cancers, the origins of NB can be linked back to defects in key cell signaling pathways during embryonic development[8]. NB originates from trunk neural crest (NC) progenitors that are committed to give rise to the sympathetic nervous system[4,8]. NC cells are a transient population of multipotent cells that, in the developing embryo upon an epithelial to mesenchymal transition (EMT), delaminate, migrate and differentiate into a broad lineage repertoire[9].

TWIST1/2 transcription factors are among the master regulators of the EMT process[10,11]. TWIST1/2 are highly conserved and guide developmental programs including cell lineage determination and differentiation, and are essential for organogenesis[10,12]. In humans, germline mutations of the TWIST1 gene are responsible for the Saethre-Chotzen syndrome (SCS), characterized by limb abnormalities, facial dimorphism, and premature fusion of cranial sutures[13]. Reactivation and aberrant functions of TWIST1/2 have been found in several carcinomas. Both TFs provide cells with critical properties including self-renewal capabilities, resistance to oncogene-induced failsafe programs and invasive capabilities thus promoting cancer initiation and progression toward a metastatic disease[10,11,14]. Since TWIST1/2 are active in NC cells, where they play a key role in driving EMT and migration, the study of their functions in NB is particularly important to better understand the neuroblastomagenesis, as distant metastases are already present by the time of diagnosis for the disseminated forms of this disease. So far, the role of TWIST1/2 in NB is still largely unknown. Upregulation of TWIST1 is found in NB with MNA and in a subset of no-MNA tumors, overexpressing MYCN or MYC[15-17]. In addition, TWIST1 protects NB cells from the pro-apoptotic effects mediated by MYCN, through the inhibition of the ARF/p53 pathway and cooperates with MYCN in NB to uphold both *in vitro* cell proliferation and *in vivo* tumor growth[15,18]. Recently, TWIST1 was also identified as a key regulator of MYCN-driven gene regulation through their cooperative binding on enhancers[18].

In this study, we initially revealed the correlation between the expression of TWIST1 and NB clinical prognostic factors *in silico* on primary NB gene expression datasets and in tumor tissue microarrays. Using an *in vivo* model for transcriptomic analyses, we then unveiled the impact of CRISPR/Cas9-mediated TWIST1 silencing on NB tumor growth, metastatic dissemination and the reorganization of the tumor microenvironment (TME).

Results

High levels of TWIST1 RNA expression are associated with poor outcomes in patients with NB.

In silico analysis using the CCLE database (https://portals.broadinstitute.org/ccle) shows that NB displays the highest levels of TWIST1 expression among 40 cancer cell lines, whereas TWIST2 is barely detected (Supplementary Fig. 1a). To further evaluate whether the expression levels of TWIST1/2 correlate with patient outcomes and NB prognostic factors, we analyzed two large clinical cohorts of primary NB tumors using the R2: Genomics Analysis and Visualization Platform (http://r2.amc.nl) (SEQC[19], n = 498; Kocak[20], n = 649). In both datasets, a high level of TWIST1 transcript strongly correlates with both a reduced overall survival (OS) (Fig. 1a; Supplementary Fig. 1b) and event-free survival (EFS) (Supplementary Fig. 1c).

Moreover, the expression of TWIST1 was more elevated in MNA NBs compared to those without MNA (Fig. 1b, Supplementary Fig. 1d); and in higher stage tumors (stages 3 and 4 vs 1 and 2; stage 4 vs 4s) (Supplementary Fig. 1e).

To understand whether TWIST1 could be a prognostic factor in NB, we stratified patients of the SEQC dataset according to the level of TWIST1 expression and either the MYCN status (Fig. 1c) or risk (HR vs low-risk (LR); Supplementary Fig. 1f). For MNA or HR patients, TWIST1 expression level had no impact on the EFS. Conversely, for no-MNA and LR cases, a high level of TWIST1 expression was associated with a reduced outcome, likewise the MNA or the HR status, hinting to a possible role for TWIST1 as a prognostic factor for these patients. As opposed to TWIST1, in the two same datasets, higher levels of TWIST2 were associated with both a better OS and EFS in NB patients (Supplementary Fig. 1g). Moreover, TWIST2 expression was increased in no-MNA NB (Supplementary Fig. 1h).

TWIST1 expression patterns reveal a correlation with poor prognostic factors in NB.

We examined the expression levels of TWIST1/2 proteins in a NB tissue microarray (TMA) (Table 1). In control sympathetic ganglia (SG), TWIST1 was not detected while TWIST2 was present with moderate intensity in 46% of SG (Fig. 2a; Table 1). TWIST1 expression was statistically significantly higher in tumors associated with poor prognosis: stages 3-4 vs stages 1-2; stage 4 vs 4s; tumors with MNA vs no-MNA; and in patients older than 18 months at the diagnosis (Fig. 2b; Table 1). On the other hand, the expression of TWIST2 was higher in tumors with better prognosis: stages 1-2 vs stages 3-4 and in patients with no-MNA vs MNA (Fig. 2b; Table 1). However, no statistically significantly differences in TWIST2 expression were observed in stage 4s vs stage 4 or in relation with age at diagnosis (Fig. 2b). Finally, TWIST1 was frequently expressed in metastases (76% positive, median score=0.95), while TWIST2 expression was uncommon (30% positive, median score=0.31) (Fig. 2a; Table 1).

TWIST1 KO impairs the neurosphere-forming ability of NB cells.

To investigate the contribution of TWIST1 in the aggressive features of NB, three cell lines, either MNA (LAN-1 and SK-N-Be2c) or non-NMA (NB-1), were chosen for a TWIST1 knockout (KO) through CRISPR/Cas9. A complete KO of the wild type (wt) TWIST1 protein expression was obtained with the sgTWIST1 #1 for the three cell lines that from now on will be referred to as sgTWIST1 cells (Supplementary Fig. 2a, b). TWIST1 KO did not significantly affected the 2D growth property of NB cell lines (Supplementary Fig. 2c), however it reduced the neurosphere-forming ability of the three NB cell lines (Fig. 3a). Consequently, the number of sgTWIST1 cells recovered from primary neurospheres was statistically significantly lower compared to Control cells (Fig. 3a), indicating the role played by TWIST1 in propagating a highly tumorigenic subpopulation of NB cells.

TWIST1 KO delays tumor growth of NB xenotransplantation and extends survival in mice.

Next, we investigated the contribution of TWIST1 in the tumorigenicity of NB cells. In three independent experiments, athymic Swiss nude mice were injected with the SK-N-Be2C Control and sgTWIST1 cells either orthotopically (500'000 cells for ortho_1 and 50'000 cells for ortho_2) or subcutaneously *(*sc*,* 250'000 cells). In all the three models, the growth of the sgTWIST1 tumors was severely delayed compared to Controls thus extending sgTWIST1 mice survival (Fig.3b, Supplementary Fig. 3a). In particular, in the first orthotopic experiment (ortho_1), 26 days after the injection, tumors in Control mice were already above the pre-determined volume for sacrifice while in the sgTWIST1 mice they were still in the lag phase (Fig. 3c). In the second orthotopic experiment (ortho_2), we observed a significant delay in the time of both SK-N-Be2c-sgTWIST1 tumor initiation and tumor growth (Fig.3d). Furthermore, 25 days after sc injections, the size of Control tumors was ~10 times larger than sgTWIST1 tumors. The latter required four additional weeks before reaching the size limit for sacrifice (Supplementary Fig.3b). Finally, in both orthotopic experiments we observed SK-N-Be2c-Control tumors invading the vena cava (n=3/6: ortho_1; n=3/8: ortho_2) (Supplementary Fig. 3c), whereas no invasion was detected in the sgTWIST1 mice group.

TWIST1 KO diminishes the malignant phenotype of tumors and decreases intrapulmonary macrometastasis

In both orthotopic *in vivo* models, Control tumors presented histological features corresponding to undifferentiated or poorly differentiated cells, while sgTWIST1 tumors were more differentiated (Fig.4a). Moreover, Control cells showed a lower degree of cohesion and a higher degree of immune cell infiltration compared to the sgTWIST1 tumors (Fig. 4a). We analyzed the effects of TWIST1 KO on the pattern of collagen III/reticulin fibers, which contribute to the ECM. Throughout all the three *in vivo* models, in Control tumor tissues the continuity of the reticular fiber framework was lost in extensive tumor areas, and we observed irregular thickening and fraying of fibers mainly at the borders of tumors (Fig. 4b, Supplementary Fig. 4a). In contrast, the sgTWIST1 tumors were characterized by a preserved reticulin mesh, resembling that of the normal adrenal gland (AG) (Fig. 4b, Supplementary Fig. 4a). This effect was not altered by the tumor size at the sacrifice (Supplementary Fig. 4b).

We speculated that the abovementioned ECM modifications associated with the expression of TWIST1 could be responsible for a "pro-neoplastic" stromal phenotype, offering less resistance for the invasive cells to escape the primary tumor site and form metastasis[21]. Therefore, the lungs of the ortho_2 experiment mice were stained by H&E and anti-mCherry for the presence of intrapulmonary metastasis (Fig. 4c). We could observe a decrease in the number of intrapulmonary micrometastases (area (A) <1000 μm2) in the sgTWIST1 group, though this

difference was not statistically significant (Fig. 4d). Conversely, the number of intrapulmonary macrometastases (A> 1000 µm2) in the sgTWIST1 mice was statistically significantly reduced (Fig. 4d) as a single one was detected in only 1/10 sgTWIST1 mouse ($2.3x10^3$ μm^2) (Fig. 4c, lower panel), whereas 6/8 Control mice had multiple macrometastases (mean macrometastases size/mice: $5.1x10^5 \mu m2$).

Identification of distinct transcriptional program regulated by TWIST1 and MYCN in NB cells

Transcriptomic analyses of SK-N-Be2c-Control and –sgTWIST1 cells and their derived-ortho_1 tumors were performed by RNAseq. Principal Component Analysis (PCA) revealed a high degree of segregation of the transcriptomic profiles of Control and sgTWIST1 for both cells and ortho_1 tumors, enabling the accurate identification of genes that are differentially expressed (DE) (Fig. 5a). We identified 2342 DE genes (1401 up- and 941 down regulated) in SK-N-Be2c cells (Supplementary Fig. 5a; Supplementary Data 1) and 2013 (1003 up- and 1010 down regulated) in the SK-N-Be2c ortho_1 tumors (Fig. 5b; Supplementary Data 1), with 1213 found in common (Supplementary Data 1). Gene ontology (GO) analyses for the DE genes in cells and in tumors reported a number of significantly enriched terms related to signaling, nervous system development, migration, proliferation, ECM organization and adhesion for both biological processes (BP) and cellular components (CC) (Fig. 5c; Supplementary Fig. 5b; Supplementary Data 2).

As downregulation of MYCN was observed upon transient TWIST1 silencing in SK-N-Be2c, a decrease in MYCN expression level could be, in part, responsible for the deregulation of the transcriptional program observed in our ortho tumors[18]. To exclude this possibility, we analyzed the expression level of MYCN protein by immunoblotting in tumors coming from the three in vivo experiments. In all sgTWIST1 tissues, we detected an increase in the level of MYCN protein compared to the Control counterpart (Supplementary Fig. 5c) although this increase was not sufficient alone to promote and sustain a more aggressive phenotype in the sgTWIST1 tumors.

To compare the transcriptional program defined by TWIST1 with the one induced by MYCN in SK-N-Be2c cells, we reanalyzed RNAseq data obtained upon MYCN shutdown using the BET-bromodomain inhibitor JC1[18]. GO analyses performed on DE genes highlighted an enrichment of gene sets mainly involved in the regulation of cell cycle and the DNA replication for both BP and CC, thus suggesting distinct functions for the two TFs (Fig. 5d; Supplementary Fig. 5d; Supplementary Data 3 and 4).

A TWIST1-mediated gene expression signature is associated with poor outcome in NB

We combined our ortho_1 transcriptomic analysis with RNAseq data of primary NB tumors to identify a TWIST1-associated gene signature relevant in primary NB. Using the 'R2 Platform, we first listed the genes either correlated (R positive) or anti-correlated (R negative) with TWIST1 expression in the SEQC dataset of NB tumors (n=7737 genes with R absolute value >0.225, Supplementary Fig. 6a). Second, we crossed this list of genes with the 2011 DE genes between SK-N-Be2c-Control and -sgTWIST1 tumors, either up- (FC positive) or down-regulated (FC negative) by TWIST1. We found 763 genes in common (Fig. 6a; Supplementary Data 5) among which we selected those that had both R and FC either positive (172 genes) or negative (317 genes). We called these resulting 489 genes the TWIST1-signature (Fig. 6b; Supplementary Data 5). Using the same SEQC dataset, we analyzed the clinical significance of the signature, and observed that genes correlated with TWIST1 in NB patients and upregulated by TWIST1 in ortho_1 tumors (R and FC positive) mostly had an elevated level of expression in high-risk, more advanced stages and MNA tumors. In addition, these tumors displayed a low level of expression of genes downregulated in the TWIST1-signature (Fig. 6c). Finally, an elevated expression level of the TWIST1-signature was associated in the SEQC and Kocak datasets with a poor OS and EFS for both the complete patient cohorts and the sub-cohorts without MNA (Fig. 6d, 6e; Supplementary Fig. 6 b, 6c).

Among the top deregulated genes in the TWIST1-signature, several have crucial roles during embryonic development, in particular for the correct development of the nervous system (*BMP7*, *FGF2*, *DTNA*, *MATN2*, *PCDHA1*, *PMP22*, *SCL1A3*). Moreover, most of the top up-regulated genes are involved in the organization of both TME (*PDGFRA*, *VCAN*, *BMP7*, *FGF2*) and ECM (*ADAMST19*, *PCOLCE*); in the EMT process (*BMP7*, *TRIM28*), as well as in cell proliferation (*FGF2* and *PDGFRA*) and apoptosis (*BMP7*) (Fig. 7a). Besides, among the top genes down-regulated in the TWIST1 signature, some are involved in neuronal differentiation (*PIRT*), and various are tumor suppressor genes (*SYT13*, *FAM134B*, *PMP22*, *C7* and *MATN2*) Fig. 7a). Several transcripts belonging to the TWIST1-signature were chosen, based on their degree of differential expression and their biological function, for validation by RT-qPCR and WB/IHC. We confirmed that *VCAN*, *PDGFRA*, *TRIM28*, *PCOLCE* and *ADAMTS19* genes were upregulated by TWIST1, as their RNA and/or protein expression levels were increased in SK-N-Be2c-Control relative to -sgTWIST1 tumors, while the opposite was true for the genes downregulated by TWIST1 (*PIRT* and *SYT13*) (Fig. 7b-d; Supplementary Fig. 7a, 7b; Supplementary Fig. 8a-c).

TWIST1 alters the level of expression of genes involved in tumor-stroma crosstalk.

Cancer cells establish a reciprocal intercellular signaling network and communicate with stromal and immune cells via the production of soluble paracrine factors and their cognate

receptors. This complex signaling network shapes the TME to sustain cancer cell proliferation and invasion. To address whether TWIST1 alters the expression of factors involved in cell-cell communication, DE genes annotated as cytokines, chemokines, growth factors, inflammatory mediators and their receptors, as well as integrin and their ligands were extracted from SK-N-Be2c tumor transcriptome. This TWIST1-tumor-stroma signature is composed by 77 DE genes, 33 up- and 44 down-regulated (Fig. 8a, Supplementary Data 6). Several play a pivotal role in the regulation of focal adhesion (*EGFR*, *ITGA11*, *ITGA6*, *PDGFRB*); cell migration (*COL5A1*, *ITGAV*, *ITGB3*, *PDGFRB*, *TGFB1*); proliferation (*FGF1*, *FIGF*, *IFI16*); angiogenesis (*ACKR3*, *ACVRL1*, *EGFL7*, *FGF1*, *FGFR2*, *FIGF*); and inflammatory and immune responses (*NGFR*, *TNF*, *TNFRSF1A*, *TNFRSF1B*, *TNFRSF4*, *TNFRSF9*, *TNFSF12*, *TNFSF13*, *TNFSF4*). A high level of expression of the TWIST1-tumor-stroma signature was associated with a poor OS and EFS of NB patients both in the SEQC (Fig. 8b) and the Kocak dataset (Supplementary Fig. 9a).

To validate the tumor-stroma signature at the protein level and further characterize TWIST1-mediated alterations in cell-cell communication, we analyzed the secretome of SK-N-Be2c-Control and -sgTWIST1 cells *in vitro* by HPLC/Tandem MS using their conditioned media (CM) containing both secreted proteins and extracellular vesicles released by tumor cells. These secretomes contained 673 DE peptides (304 up- and 369 down-regulated) (Fig. 8c; Supplementary Data 7) that corresponded to 678 genes. GO analyses revealed an enrichment of BP linked to nervous system development, signaling, response to stimuli, migration, and proliferation (Supplementary Fig. 9b; Supplementary Data 8).

Crossing secretome and transcriptome data from both cells and tumors, we identified 131 commonly deregulated terms, whereas 75 and 55 were uniquely shared between the secretome and either the cell or tumor transcriptome, respectively (Fig. 8d; Supplementary Data 7). Finally, after crossing the TWIST1-tumor-stroma signature with the secretome of cells, we could identify 17 commonly DE terms, among which 14 were also found to be in common with the transcriptome of cells (Fig. 8e). Most of the commonly deregulated terms were up regulated by TWIST1 and annotated as growth factors, and for all terms but *COL5A1* and *VGF*, the impact of TWIST1 on RNA and protein expression was always found to be correlated.

Myofibroblast-associated gene expression is reduced in the stroma of sgTWIST1 orthotopic tumors.

Among the terms deregulated in the abovementioned tumor-stroma signature, several are also known for being involved in the crosstalk between cancer cells and the resident and recruited stromal cells (i.e. *TGFB1*, *HGF*, *FGF*, *FGFR*, *EGFR*, *PDGFR*, *CXCL12*) and thus they could mediate a TME sustaining the tumor growth[22]. One of the main stromal changes within a pro-

tumorigenic TME is the appearance of cancer-associated fibroblasts (CAFs), playing a critical role in arranging the "soil" within which tumor cells proliferate[23]. To verify whether we could detect the presence of CAFs in the tumor stroma, the ortho_1 RNAseq data were aligned with the murine genome. Between Control and sgTWIST1 tumors, 89 stromal genes were found to be DE(69 up- and 20 down-regulated) (Fig. 9a; Supplementary Data 9). Genes up-regulated in the stroma of TWIST1 expressing Control tumors showed a significant enrichment of muscle contraction-related terms (Fig. 9a; Table 2). This was defined as the myofibroblastic signature (n=36 genes) according to the literature[24-27]. GO analysis for the murine DE genes reported a number of statistically significantly enriched terms related to sarcomere organization and muscle contraction (Fig. 9b, Supplementary Data 10), supporting a TWIST1-mediated recruitment and activation of myofibroblasts.

Besides, among the up-regulated genes, we noticed the Macrophage Receptor with Collagenous Structure (Marco), which defines a subtype of alternatively-activated M2 tumor-associated macrophages (TAMs) with immunosuppressive functions and involved in tumor progression[28]. Six up-regulated genes of the myofibroblastic signature (*Pvalb*, *Neb*, *Acta1*, *Ttn*, *Myh1*, *Msln*) (Supplementary Fig. 10a) and *Marco* were confirmed by RT-qPCR. For the selected genes of the signature, a reduction in their RNA expression levels was observed in both ortho_sgTWIST1 tumor stroma only, and were undetectable in the tissues from the sc tumors (Fig. 9c, Supplementary Fig. 10b). The reduced RNA expression level of *Marco* in sgTWIST1 tumor stroma was validated in all the three *in vivo* models (Fig. 9c, Supplementary Fig. 10b). Finally, qualitative validation by IHC with the CAF marker fibroblast-activation protein (Fap) confirmed the presence of CAFs in both Control and sgTWIST1 ortho_1 tumors (Fig. 9d).

To analyze the potential interactions existing between the TWIST1-associated tumor-stroma signature and the DE stromal genes, a protein-protein interacting (PPI) network was constructed using the STRING website (https://string-db.org/).The two groups of DE genes clustered separately and had a high level of linkage both among genes of each category and reciprocally (Fig. 10). Two stromal genes reported as myofibroblastic markers, *Acta1*, belonging to the actin family and *Actn2*, a member of the spectrin superfamily, were strongly linked to the network of myofibroblastic genes and connected with the tumor gene cluster, via *TGFB1*, *TGFB3*, *HGF*, *LAMC3* and *LAMA5*, *FIGF* and *HSPB1*[29,30].

Discussion

In this study, we discovered a role for the embryonic TFs TWIST1 and TWIST2 as prognostic factors in NB. We could reveal the contribution of TWIST1 in enhancing primary and secondary tumor growth and in mediating an aggressive phenotype in *in vivo* NB xenografts. Furthermore, we identified a TWIST1-associated transcriptional signature, which correlated with outcomes in human primary tumors and activated the TME in an orthotopically-derived xenograft murine model.

TWIST1 and TWIST2 have previously been described as playing a distinct role during embryonic development and having anti-correlated transcriptional expression patterns in spontaneous focal mammary tumors in mice and in human melanoma, colon, kidney, lung and breast cancer[31]. In this study, we show their opposite expression pattern in primary NB and their antithetical prognostic value, highlighting that theTWIST1 expression was correlated with unfavorable NB prognostic factors, metastasis and poor survival. These findings are in line with prior studies conducted on non-pediatric cancers showing the overexpression of TWIST1 in high grade and invasive/aggressive breast, bladder, cervical, ovarian and hepatocellular cancers where it might also serve as prognostic factor for poor survival[32]. Moreover, we confirmed previous data showing the association of TWIST1 with MNA NB on larger cohorts of patients[15,16]. Furthermore, TWIST2 was mainly detected in normal tissues and in NB with better prognosis. These results are in contrast with those obtained by others, showing an association between the upregulation of TWIST2 and a more aggressive tumor phenotype[33-36]. Importantly, we identified TWIST1 as a valid candidate in predicting the poor outcome of patients with no-MNA or LR NB, in the same way as the amplification of MYCN or the HR classification.

Our *in vivo* investigations on the biological effects of TWIST1 reveal that its loss delays the primary tumor initiation and growth of NB, regardless of the number of cells and the injection site. These data are aligned with prior evidence showing that the suppression of TWIST1 hampers the growth of primary skin papilloma induced by carcinogens[37]; and that the pharmacological inhibition of the Twist-BRD4-Wnt5a signaling axis results in the reduction of tumorigenicity of basal-like breast cancer[38]. Moreover, the overexpression of TWIST1 accelerates tumor establishment and growth of MCF-7-derived breast cancer and transforms mouse embryonic fibroblasts in cells with high tumorigenic potential[31,39]. In contrast with these findings, TWIST1 was shown as nonessential for primary tumor initiation and growth in several *in vivo* murine models for breast cancer, pancreatic ductal adenocarcinoma and hepatocellular carcinoma, although it seems to play a pivotal role in driving cells migration and invasion[14,40,41]. Taken together, these antithetical findings suggest that the role of TWIST1 in carcinogenesis might depend upon the tumor settings as well as on oncogenic drivers.

In our experiments, TWIST1-expressing tumors displayed a phenotype typical of less differentiated NBs. Additionally these tumors were characterized by abundant fascicules of spindle-shaped cells, typical of a mesenchymal-like morphology. The role played by TWIST1 in driving the EMT and in maintaining cells in a mesenchymal state has been widely documented as part of both the morphogenesis during embryonic development, and in the pathogenesis of multiple types of invasive cancers[41-44]. Moreover, several studies demonstrate an association between the EMT and the acquisition of stem-like characteristics in normal and neoplastic epithelial tissues, identifying in TWIST1 the molecular linker between these two biological processes[45-47]. In our study, TWIST1-expressing NB cells were able to grow *in vitro* as neurospheres, known to be enriched in tumor-initiating cells (TIC) exhibiting stem-like features[48]. Furthermore, our data reveals a role for TWIST1 in metastatic dissemination in NB, as an increase in the number and in the size of pulmonary metastases was observed in Control mice. In fact, the decrease of the invasive mesenchymal-type cells in the sgTWIST1 tumors and the reduced ability of sgTWIST1 cells to maintain the TIC population could at least in parts explain the reduction in the number of pulmonary micrometastases observed in sgTWIST1 mice. Moreover, the suppression of TWIST1 also had an impact on the last step of the metastatic cascade, the colonization, consisting in the growth of micrometastases into macroscopic metastases, that lies on the self-renewal capability and the proliferative potential of invading cells.

The ECM is another key player in promoting tumor invasion and metastasis. Disruption and stiffness of this framework has been demonstrated to contribute to malignant transformation and cancer progression by destabilizing the cell–cell adhesions and promoting cell invasion[21,49]. In Control tumors expressing TWIST1, we observed a disruption of the reticulin mesh, one of the main components of the ECM, and an increase in their density along the tumor border. In contrast, sgTWIST1 tumors preserved a nest-like arrangement of thin reticular fibers, as observed in the normal adrenal gland. Interestingly, a disorganized and cross-linked reticulin network was associated with poor NB prognosis, and a morphometric classification based on variations of both blood vessels and reticulin fibers shape and size was proposed to identify ultra-high risk NB patients[50]. The involvement of TWIST1 transcriptional targets in the degradation/remodeling of the ECM has been demonstrated in both normal embryonic development as well in cancer[21,42,51-53]. In our orthotopic model, we found several genes involved in the organization of the ECM and the TME, such as *VCAN*, *ADAMTS19*, *PDGFRA*, *TRIM28* and *PCOLCE*, among the top 20 upregulated by TWIST1, suggesting a role for TWIST1 in defining a permissive microenvironment contributing to the survival and maintenance of cancer stem-like cells. *PCOLCE* is a direct transcriptional target of TWIST1 and is implicated in the regulation of collagen deposition during both early craniofacial

development and in osteosarcoma, where it promotes tumor growth, cell migration and invasion[42,54] . In our study using two cohorts of primary NB, *PCOLCE* was the gene presenting the highest correlation with TWIST1 expression regardless of the amplification status of MYCN, suggesting a role for TWIST1 in the control of *PCOLCE* expression also in primary NB.

For the first time, we identified a NB-associated TWIST1-signature by combining the transcriptomic data of orthotopic tumors with that of primary tumors. Importantly, an elevated expression of this signature was found in MNA and HR tumors, and it was associated with poor survival in the entire NB datasets and their sub-cohorts without MNA. In addition, a subgroup of TWIST1-target genes involved in shaping the interface between tumor cells and its stroma could be extracted, which we named TWIST1-tumor-stroma signature. Both signatures induced by TWIST1 were linked to poor survival *in silico*, indicating their biological relevance and confirming the functional role of TWIST1 in NB pathogenesis.

The cooperation between TWIST1 and MYCN in defining a transcriptional program in NB supporting *in vitro* cell proliferation and *in vivo* tumor growth has already been shown[15,18]. Using our results and previous published findings on NB, we conclude that these TFs seem to orchestrate distinct functions. Indeed, GO analysis on our transcriptomic data revealed that suppression of TWIST1 in SK-N-Be2c cells and tumors mainly deregulated pathways involved in signaling, nervous system development, migration, adhesion, ECM organization, and cell proliferation. Interestingly, these pathways were also principally deregulated by the genes enriched in the TWIST1-signature. On the other side, GO analysis performed on RNAseq data of SK-N-Be2c cells downregulated for MYCN through JC1[18] highlighted a major role for MYCN in controlling the cell cycle regulation and DNA replication. Similar pathways were also identified upon MYCN silencing through JC1 or shRNA in MNA NB cell lines [55], thus confirming a predominant role for this TF in supervising mostly the proliferation of cells.

There are several limitations in our study. First, the use of only one NB cell line to obtain our *in vivo* model could represent an issue in the wider relevance of our findings. Although SK-N-Be2c cells are commonly used for NB research, they in fact might not fully represent the biology and diversity of the disease itself. Thus, our observations about the role of TWIST1 in enhancing NB tumor aggressiveness remain to be verified using NB cell lines without MNA as well as primary NB cells. Second, RNAseq analysis was performed on tumors of the ortho_1 experiment, which did not give rise to macroscopic metastases. This was probably caused by extremely rapid tumor growth, which might have prevented the formation of macrometastases. However, this model is suitable for appreciating the effects of TWIST1 on tumor growth capacity and phenotypic features as well as on TME remodeling. Moreover, the main deregulated genes and pathways were consistently altered by TWIST1 between SK-N-Be2c

cells and ortho_1 tumors, and the most relevant genes were confirmed in the ortho_2 tumors. Importantly, the biological relevance of the transcriptional program defined by TWIST1 in the SK-N-Be2c ortho_1 xenografts were validated in human primary NB, with the identification of a TWIST1-associated signature and a tumor-stroma signature, both displaying a strong prognostic impact in two cohorts of NB patients. Third, in our study we only focused on the incidence of metastases in the lungs of mice, which occurs in approximately 4% of children with newly diagnosed NB[56]. We did not detect macrometastases in the liver, one of the most frequent sites of infiltration in children together with bone marrow, bone, and lymph nodes. Fourth, the unambiguous identification of the stromal counterpart activated by the tumor-stroma signature remains challenging. Our transcriptomic data suggest an enrichment of M2 TAM and of myofibroblasts, the most abundant stromal cells supporting tumor progression, in TWIST1-positive xenografts. The marked connection observed between the TWIST1-tumor-stroma signature and the stromal DE genes by STRING analysis further support their role in mediating the NB-associated alterations in the tumor stroma. However, the qPCR validation of the stromal genes belonging to the myofibroblastic signature was hampered by sometimes extremely low/undetectable expression levels. This was probably due to the very limited number of stromal cells present in whole tumor lysates. Single cell sequencing could further facilitate the characterization of the impact of TWIST1 on stroma composition. Moreover, it could be argued that an immunocompromised mouse model does not represent the most suitable setup to study TME components. Genetically engineered models spontaneously developing tumors or humanized mouse NB models could represent other valid alternatives to recapitulate the TME composition in NB[57]. Finally, precisely identifying CAF by IHC remains difficult due to the lack of specific myofibroblast markers, a common issue in all studies.

In summary and for the first time, our study revealed the prognostic significance of TWIST1 and TWIST2 in NB. The biological impact of TWIST1 on tumor growth and metastatic formation capacity was associated with alterations in the ECM composition and with the establishment of a TME supportive of tumor growth and progression. The transcriptional program activated by TWIST1 in our *in vivo* model of NB further supported these findings and its validation in primary NB unveiled a correlation with HR disease and poor prognosis. All our findings strongly indicate a very promising role for targeting TWIST1 in the therapy of HR or relapsed/refractory NB, which remains an almost universally fatal disease.

Methods

Cancer Cell Line Encyclopaedia (CCLE) database analysis

The CCLE database (https://portals.broadinstitute.org/ccle) was used to compare the mRNA expression level of TWIST1 and TWIST2 in a range of 36 different cancer types (Affymetrix arrays: Affimetrix Human Genome U133, Plus 2.0). Quality filtering and normalization were performed using Robust Multi-array Average (RMA) and quantile normalization.

Tumor Microarray (TMA) and Immunohistochemistry

The TMA was composed by 72 primary tumors, 25 matched metastases and 44 matched control normal tissues (13 sympathetic ganglia and 31 adrenal glands) (Table 1) obtained from 72 patients diagnosed with NB between July 1988 and November 2001 treated and followed at the Bicêtre hospital (Le Kremlin-Bicêtre) and the Gustave Roussy Institute (Villejuif). Immunohistochemical study on patient tissues was performed after patients' informed consent and according to the ethical regulations of the institution. On average, 4 tissue cores with a 0.6 mm diameter were obtained and transferred into a recipient paraffin block using a tissue arrayer (Alphelys: Beecher Instruments Micro-Array Technology, Plaisir, France). TMA sections 5-µm were made on Benchmark XT Ventana (ROCHE Diagnostics). After dewaxing, antigen retrieved is performed using water-bath heating in the following buffers: in citrate buffer pH 6.0 (CC2 citrate-based buffer Ventana Medical Systems ROCHE Diagnostics) for TWIST1 and in a CC1 buffer of pH 8 (CC1 = Tris-Borate/ EDTA, Ventana Medical Systems ROCHE Diagnostics) for TWIST2. Slides were then incubated 1h at RT with the rabbit polyclonal anti-TWIST1 (1/50, ABD29, Millipore, Burlington; MA, USA); or 1h at 37°C with the sheep polyclonal anti-TWIST2 (1/200, AF6249, R&D Systems, Minneapolis, MN, USA) in Antibody Diluent Buffer from Ventana Medical Systems, ROCHE Diagnostics. The detection kit for the antibodies is the UltraView DAB detection Kit (Ventana Medical Systems Inc./ Roche Diagnostic). A counter-staining of the nuclei was used for 12 minutes by Hematoxylin. Immunostaining scores (0–4) were established for each stained tissue by semi-quantitative optical analysis by two independent investigators blinded for clinical data. The percentage of positive cells in each sample was scored as follows: 0, all cells negative; 1+, up to 25% of cells were positive; 2+, 26% to 50%; 3+, 51% to 75%; 4+, more than 75%.

Cell culture

The established human MNA NB cell lines (SK-N-Be2c and LAN-1) were obtained from their lab of origine[58,59]. Authentication of SK-N-Be2c and LAN1 cell lines was performed by microsatellite short tandem repeat analysis before starting the transduction experiments (Microsynth, Switzerland). The no-MNA NB1-M primary cells were derived in our laboratory from a bone marrow tissue recovered at the diagnosis from a patient with NB at the Hematology Oncology Unit of the University Hospital of Lausanne, Switzerland[48]. All cell lines

were cultured in Dulbecco's modified Eagle's medium (D-MEM) (Gibco, Paisley,UK), supplemented with 1% penicillin/streptomycin (Gibco) and 10% heat inactivated Fetal Calf Serum (FCS) (Sigma-Aldrich, St. Louis, Missouri, USA) and under standard culture conditions in humidified incubator at 37°C with 5% CO2.

TWIST1 knock out through CRISPR/Cas9 technology

Two sgRNAs targeting the first exon of the TWIST1 gene were chosen in the published sgRNA library[60]. Oligos were designed as follow: sgTWIST1-1: forward 5'-CACCGCGGGAGTCCGCAGTCTTACG-3'; reverse 5'-AAACCGTAAGACTGCGGACTCCCGC-3'; sgTWIST1-2: forward 5'-CACCGCTGTCGTCGGCCGGCGAGAC-3'; reverse 5'-AAACGTCTCGCCGGCCGACGACAGC-3'. The lentiviral vector lentiCRISPR v2[61] was obtained from Adgene (Cambridge, USA). LentiCRISPR v2-sgTWIST1 plasmids were constructed according to the manufacturer's instructions (Adgene), and used to transduce Control cells. Virus production and lentiviral infections were performed as previously described[62]. Transduced SK-N-Be2c, LAN-1 and NB1-M cells were selected 24 h post-infection with either 5 µg/ml for SK-N-Be2c or 1 µg/ml for LAN-1 and NB1-M cells of puromycin (Gibco). Clones were isolated by limiting dilution cloning in a 96-wells plate from the Control and sgTWIST1 #1 of LAN-1 and SK-N-Be2c cell lines. Only clones derived from a single colony were selected and further screened by Immunoblotting. To avoid potential problems caused by variability during single-cell clonal expansion, we pooled 5 and 7 clones for the Control and sgTWIST1 SK-N-Be2c cells, respectively; for the LAN-1 cells, 6 clones were pooled for both Control and sgTWIST1 cells. SK-N-Be2c-Control and sgTWIST1 pools of cells were further transduced with a lentiviral vector expressing the mCherry gene (Ex-NEG-Lv244 from GeneCopoeia™). These cells expressing the mCherry gene were used for the ortho_2 and the sc xenograft experiments. In addition, genome editing in SK-N-Be2c sgTWIST1 cells was verified by NGS sequencing. Briefly, PCR amplicons were designed across the TWIST1 genomic regions targeted by the sgRNAs to examine generation of indels. A first PCR of 20 cycles was performed using the primers Twist1-nest-F: 5'-GCAAGAAGTCTGCGGGCTGTGG-3' and Twist1-nest-R: 5'-GGATGATCTTCCGCAGCGCG-3', followed by purification with QIAquick PCR purification kit (QIAGEN). Then we run a second PCR of 10 cycles with nested primers containing Illumina overhang adapter sequences: Illumina-P5-Twist1-F: 5'-TCGTCGGCAGCGTCAGATGTGTATAAGAGACAG AAGAAGTCTGCGGGCTGTGGCG-3'; Illumina P7-Twist1-R: 5'-GTCTCGTGGGCTCGGAGATGTGTATAAGAGACAGCGCTCCCGCACGTTGGCCATG-3'. Both PCR were performed using the 2xKAPA HiFi HotStart ReadyMix as follow: 95°C for 5

minutes, 10 cycles at 98°C for 20 s, 73°C for 30 s, 72°C for 30 s; then 72°C for 5 min. Finally, a third PCR was performed to attach Illumina adaptors and barcodes to samples according to manufacturer's instructions. Amplicons were purified by using AMPure XP (Beckman Coulter, Indianapolis, USA), and sequenced with a MiSeq Micro 300 (Illumina Inc., San Diego, USA) at the Lausanne Genomics Technologies Facility (GTF) (https://wp.unil.ch/gtf). After high throughput sequencing reads, PCR amplicons were checked for indels using CRISPResso (https://crispresso.pinellolab.partners.org). The results of the sequencing of the bulk population of SK-N-Be2c-sgTWIST1 cells, the 7 derived clones, and the 4 sgTWIST1 ortho_1 tumors are shown in Supplementary Data 11. Surprisingly, in all the sgTWIST1 clones we detected the same three main indels. Note that three alleles found in the SK-N-Be2c cells, indicating a triploidy of this genomic region as previously described[63].

Neurosphere Assay

NB cells ($2x10^4$ cells/ml) were cultured in Neural Crest Stem Cell culture medium (NCSC) [DMEM/F12 (Gibco) supplemented with 1 % penicillin/streptomycin (Gibco), 2 % B27 (Gibco), 20 ng/ml human recombinant bFGF (Peprotech, Rocky Hill, USA), 1% N2 (Gibco), 2-Mercaptoethanol 50µM (AppliChem, Darmstadt, Germany) 15% Chicken Embryo Extract, 20 ng/ml IGF-1 (Peprotech), Retinoic Acid 110 nM], using poly-Hema-coated six wells plates to prevent cell adhesion. After 7 days in culture, pictures of sphere were taken using an Olympus IX53 inverted microscope (Olympus, Shinjuku, Japan) and acquired with the Olympus cellSense imaging software. Spheres were dissociated with StemPro Accutase Cell Dissociation Reagent (Gibco, A11105-01) and the number of cells recovered after the dissociation of spheres was determined using the trypan blue exclusion method.

Proliferation assay

Briefly, $1.2*10^4$ MNA (SK-N-Be2c and LAN-1) and $3*10^4$ no-MNA (NB1-M) cells were seeded in quadruplicate in 96-wells plate in DMEM/FCS. Cell proliferation was assessed using the CellTiter 96® Aqueous Non-radioactive Cell proliferation Assay (Promega, Madison, WI, USA) according to the manufacturer's protocol.

***In vivo* studies**

Animal experiments were carried out with athymic Swiss nude mice (Crl:NU(Ico)-Foxn1^{nu}; Charles River Laboratory, France) in accordance with established guidelines for animal care of the Swiss Animal Protection Ordinance and the Animal Experimentation Ordinance of the Swiss Federal Veterinary Office (FVO). Animal experimentation protocols were approved by the Swiss FVO (authorization numbers: VD2995 and VD3372). All reasonable efforts were made to reduce suffering, including anesthesia for painful procedures. For surgical procedures, mice were anaesthetized using isoflurane (Baxter, Deerfield, IL, USA) and received

paracetamol as analgesia the day before the surgery. Orthotopic implantations were performed as previously described[64] with slight modifications: $5x10^5$ (ortho_1, 6 mice/group) and $5x10^4$ (ortho_2, 12 mice/group) SK-N-Be2c cells were resuspended in 10 µl of PBS and injected in the left adrenal gland after a small incision above the left kidney. Tumor growth was followed by ultrasound every 7 to 14 days at the Cardiovascular Assessment Facility (University of Lausanne). For subcutaneous implantation, groups of 5 mice were injected in the right flank with $2.5x10^5$ cells suspended in 200 µl 1:1 mix of DMEM and BD Matrigel™ Basement Membrane Matrix (BD Biosciences, Bedford, MA, USA). The grafted animals were then weekly monitored with calipers for tumor growth assessment. The tumor volume was calculated using the formula: volume = 4/3 × π × (depth × sagittal × transversal)/6 for ortho tumors; and volume = (length x width^2)/2 for sc tumors. For both orthotopic and subcutaneous implantations, mice with tumor volumes around ~1000 mm^3 were sacrificed using CO_2. Tumors and organs (lungs, liver) were cut into pieces and snap frozen in liquid nitrogen or fixed in formol and embedded in paraffin (lungs, liver, kidneys and spleen).

RNA isolation

Total RNA from cell lines and tumors was extracted using RNeasy kit (Qiagen, Hilden, Germany). RNA concentration was quantified using a Nanodrop (Agilent Technologies, Wilmington, DE, USA). For the RNA sequencing, RNA was quantified using Qubit Fluorometer (Life Technologies, Carlsbad, CA, USA).

RNAseq library preparation

RNAseq was performed at the iGE3 Genomics platform (University of Geneva, https://ige3.genomics.unige/ch) using standard techniques RNA integrity was verified using the Agilent 2100 Bioanalyzer system (Agilent Technologies). The total RNA ribo-zero gold kit from Illumina was used for the library preparation with 1 µg or 500 ng of total RNA as input for cells (n=3 biological replicates/group) and tumors (n=4/group), respectively. Library molarity and quality were assessed with the Qubit and Tapestation using a DNA High sensitivity chip (Agilent Technologies). Libraries were pooled at 2 nM and loaded for clustering on 1.5 lanes for cells and 1.5 lanes for tumors of a Single-read Illumina Flow cell. Reads of 100 bases were generated using the TruSeq SBS chemistry on an Illumina HiSeq 4000 sequencer.

Bioinformatics analysis of RNAseq data

For all samples, fastq files with 100 nucleotides long single-end reads were mapped with STAR version 2.5.2b on both the Human genome version Hg19 and the Mouse genome version Mm10, simultaneously. The following options were changed from the default parameters: --outSAMmultNmax 50; --outFilterMatchNminOverLread 0.4; --quantMode TranscriptomeSAM. Transcriptome annotations in gtf format for both organisms were downloaded from the

gencode website (https://www.gencodegenes.org/). Reads mapped on either the Human or the Mouse transcriptome were then parsed and split in one file per organism with an in-house perl script. Reads with matches on both Human and Mouse were discarded from the Mouse file. Per-gene counts and rpkm were then extracted independently for each organism using rsem version 1.3.0. All RNAseq per-gene data quality checks and analysis were done in R. Mouse and Human data were analyzed independently, but following the same protocol. Protein coding genes with a log2(rpkm) value above 1 in at least one sample were kept (13742 genes in SK-N-Be2c for Human data; 14538 for Mouse data). Principal Component Analysis were done using the normalized log2 (rpkm) values. Clustering analysis were performed on the normalized log2 (rpkm) values using euclidean distance measures and the ward.D2 agglomeration method. Differential analyses were performed using the raw counts in DESeq2 package version 1.26.0. For each comparison, the cutoffs for fold-change (in log2) and adjusted *p* values to call differentially transcribed genes were set to 1 and 0.05 for Human, respectively, and to 0.5 and 0.05 for Mouse, respectively. Heat maps for sample correlations and for specific gene lists were generated using the heatmap.2 function from the gplots package version 3.0.1.2 on the log2 of DESeq2 normalized counts. Functional gene ontology analysis was performed by applying a hypergeometric test on selected genes lists against gene sets from KEGG, GO (Molecular Function, Biological Process and Cellular Component), REACTOME, and BIOCARTA pathways. The *p* value cutoff for terms selection was set to 0.001 for Human data and to 0.01 for Mouse data; only those terms with an adj *p* value below 0.01 and 0.1 were taken into consideration for the graphical representation, respectively. For the GO analysis of the secretome, the lines containing multiple gene references were split before to apply the hypergeometric test on the resulting list of genes (673 terms in the secretome vs 678 terms in the transcriptome). For external RNAseq data analysis (Super series number: GSE80154; SubSeries number: GSE80153), fastq files from GSM2572350 to GSM2572355 corresponding to Be2C samples at 0 (DMSO: GSM2572350 to GSM2572352) and JQ1 24h (GSM2572353 to GSM2572355) were downloaded. These samples were then re-analyzed by applying the same protocol used for the local RNAseq data.

Real-Time qPCR

cDNA were prepared from 0.5 or 1 µg of RNA for the validation of human or murine genes, respectively using PrimeScriptTM reagent kit according to the manufacturer's instruction (TAKARA Bio Inc., St.Germain-en-Laye, France). The expression level of selected genes was validated by semi-quantitative real-time PCR using primer pairs described in Supplementary Data 12 and the QuantiFast SYBR® green kit (Qiagen, Hilden, Germany). Cycling conditions were: 5 min at 95°C, 40 cycles of 10 sec at 95°C, 30 sec at 60°C, and 1 sec at 72°C with the Rotor Gene 6000 real-time cycler (Corbett, Qiagen). Gene expression levels were determined

by normalization to either HPRT1 (human genes) or β-actin (murine genes) housekeeping genes using the ΔCt method.

Immunohistochemistry

Histopathological analyses were performed on blocks embedded in paraffin at the Mouse Pathology Facility of Lausanne University (Epalinges, Switzerland) and at the Histology Core Facility of the EPFL (Lausanne, Switzerland). Thin tumor sections (3 µm thick) were de-waxed and rehydrated and then stained with hematoxylin and eosin; Gomori's for reticulin or type III collagen detection, or IHC was performed using primary antibodies (Supplementary Data13). Staining were imaged using an Olympus BX43 light microscope and then acquired with the Olympus cellSense imaging software or using the EVOS5000 imaging system (Life Technologies); or whole slides were scanned using the NanoZoomer S60 Digital slide scanner C13210 (Hamamatsu, Japan) at the 20x magnification with a resolution of 0.46 µm/pixel. Visualization and analyses of the scans was performed using the QuPath imaging software (https://qupath.github.io). For the quantification of VCAN and α-mCherry, the entire surface either of the tumor or of three subsequent lung sections separated by a depth of 100 µm has been taken into consideration, respectively. Quantification was perfomed with the QuPath software according to the following pipeline: select a region of the tumor (magnification: 12.48X), analyze, cell analysis, positive cell detection. Options modified from the default parameters: image type: Brightfield (other); detection image: optical density sum; intensity threshold parameters: threshold 1+: 0.3.

Immunoblotting

NB cells and SK-N-Be2c-derived ortho tumors were lysed in NP40 buffer (50 mM Tris-HCl pH 8.0; 150 mM NaCl; 1% NP-40 and 1x protease inhibitor cocktail (Complete mini, EDTA-free, Roche, Mannheim, Germany). Cell lysates were centrifuged at 15'000 rpm at 4°C for 10 min. Supernatants were recovered and protein concentrations were measured using Bradford method (Bio-Rad Laboratories, Hercules, CA, USA). Equal amount of total protein lysate (40 µg for DE genes validation; 50 µg for TWIST1 and MYCN validation) was loaded onto 4-15% precast polyacrylamide Mini-PROTEAN TGX gel (Bio-Rad Laboratories). Proteins were transferred to PVDF membrane (Immuno Blot,Bio-Rad Laboratories) and blocked with 3% nonfat dry milk in TBS-T 0.1%, incubated overnight at 4˚C with primary antibodies (Suppl Table 10) and then for one hour with the appropriate secondary antibodies (Suppl Table 10). Proteins were imaged using either the WesternBright Sirius Kit or the WesternBright Quantum Kit (Advansta Inc., San Jose, CA, USA) and the Fusion FX Spectra multimodal imaging platform (Vilber Lourmat, Marne-la-Vallée, France). Quantification of immunoreactive bands was performed using the ImageJ software according to the following pipeline: analyze, gel, select

1 lane, plot lanes, manually define the area corresponding to each band, wand tool to quantify each selected area.

Protein extraction for cell secretome analysis

Three independent conditioned media (CM) samples were recovered from SK-N-Be2c Control and sgTWIST1 cells. Once cells reached ~75% of confluence, the medium was replaced with FBS- and phenol red-free DMEM (Gibco) in which cells were incubated for 24 hours. CM were first clarified by three centrifugation steps: 10' at 300 x g; 10' at 2000 x g cells; and 30' at 10000 x g at 4°C, and then concentrated using 15 ml Amicon spin filter cartridges (cutoff: 3 kDa, 10705884-Merck Millipore, Burlington, MA, USA) by serial addition of 10 ml of CM and centrifugation at 4000 x g until 1.5 ml were left. After dilution in 100 mM Ammonium Bicarbonate buffer to the starting volume, the CM were re-concentrated by centrifugation at 4000 x g, and these steps were repeated twice until 0.5 ml were left. Finally, aliquots were snap frozen in liquid nitrogen and used for the LC-MS analysis performed at the Protein Analysis Facility (University of Lausanne, Switzerland). CM were dried in a SpeedVac and then digested according to a modified version of the iST protocol [65]. Pellets were resuspended in 50 µl of modified iST buffer (2% sodium deoxycholate, 20mM DTT, 5mM EDTA, 200mM Tris pH 8.6) and heated at 95°C for 5 minutes. 50 µl of 160 mM chloroacetamide (in 10 mM Tris pH 8.6) were then added and cysteines were alkylated for 45 minutes at 25°C in the dark. After 1:1 dilution with H2O, samples were adjusted to 3 mM EDTA and digested with 0.5 µg Trypsin/LysC mix (Promega #V5073) for 1h at 37°C, followed by a second 1h digestion with a second, identical aliquot of proteases. To remove sodium deoxycholate, two sample volumes of isopropanol containing 1% trifluoroacetic acid (TFA) were added to the digests, and the samples were directly desalted on a strong cation exchange (SCX) plate (Oasis MCX; Waters Corp., Milford, MA) by centrifugation. After washing with isopropanol/1% TFA, peptides were eluted in 250ul of 80% MeCN, 19% water, 1% (v/v) ammonia.

Mass spectrometry analyses

Tryptic peptides fractions were dried and resuspended in 0.05% TFA, 2% (v/v) acetonitrile, for mass spectrometry analyses. Tryptic peptide mixtures were injected on an Ultimate RSLC 3000 nanoHPLC system (Dionex, Sunnyvale, CA, USA) interfaced to an Orbitrap Fusion Tribrid mass spectrometer (Thermo Scientific, Bremen, Germany). Peptides were loaded onto a trapping microcolumn Acclaim PepMap100 C18 (20 mm x 100 µm ID, 5 µm, 100Å, Thermo Scientific) before separation on a reversed-phase custom packed nanocolumn (75 µm ID × 40 cm, 1.8 µm particles, Reprosil Pur, Dr. Maisch). A flowrate of 0.25 µl/min was used with a gradient from 4 to 76% acetonitrile in 0.1% formic acid (total time: 65 min). Full survey scans were performed at a 120'000 resolution, and a top speed precursor selection strategy was applied to maximize acquisition of peptide tandem MS spectra with a maximum cycle time of

0.6s. HCD fragmentation mode was used at a normalized collision energy of 32%, with a precursor isolation window of 1.6 m/z, and MS/MS spectra were acquired in the ion trap. Peptides selected for MS/MS were excluded from further fragmentation during 60s.

Mass spectrometry data analysis and processing

Tandem MS data were processed by the MaxQuant software (version 1.6.3.4)[66] incorporating the Andromeda search engine[67]. The UniProt human reference proteome database of January 2019 was used (73'950 sequences), supplemented with sequences of common contaminants. Trypsin (cleavage at K,R) was used as the enzyme definition, allowing 2 missed cleavages. Carbamidomethylation of cysteine was specified as a fixed modification. N-terminal acetylation of protein and oxidation of methionine were specified as variable modifications. All identifications were filtered at 2% FDR at both the peptide and protein levels with default MaxQuant parameters. After inspection and data QC based on the iBAQ[68] values, the LFQ label-free values[69] were used for protein quantitation. MaxQuant data were further processed with Perseus software[70] for the filtering, log2-transformation, normalization of values and the statistical analyses. After removal of contaminants and reverse hits, intensity values were log2 transformed. Only proteins identified by at least two peptides and quantitated in at least all three samples of one condition were retained for further analysis. Missing values were imputed with standard Perseus parameters (normal distribution with width 0.3 and down-shifted by 1.8 SD). An unpaired T-test was used to determine significant changes, corrected for FDR with the Benjamini-Hochberg method and a threshold q-value at 0.01. Imputed values were subsequently removed from tables. Gene Ontology functional analysis were performed as previously described in the "Bioinformatics analysis" section, after splitting the lines containing multiple genes references.

Statistical analysis

All statistical analyses were performed using GraphPadPrism 8.3.0 (GraphPad Software Inc., San Diego, CA, USA). D'Agostino-Pearson normality test was performed for each data set, and depending on data distribution, they were analyzed with unpaired two-tailed parametric t-test or non parametric Mann-Whitney test to compare two different conditions.

Reporting summary. Further information on research design is available in the Nature Research Reporting Summary linked to this article.

Data availability

All data generated during this study are included in this article (and its Supplementary Information files). The RNAseq, proteomics and image corresponding datasets can be accessed at the GEO public repository using the accession number GSE160765; at the Proteomics Identifications Database (PRIDE) using the accession number PXD024200; and

at the Zenodo repository with the doi: 10.5281/zenodo.4543478, respectively. The RNAseq data of SK-N-Be2c JC1 samples were obtained from GEO, using the accession number GSE80153. The relevant data that support the findings of this study are available from the corresponding author upon reasonable request. Source data are provided with this paper.

References

1 Maris, J. M. Recent advances in neuroblastoma. *The New England journal of medicine* **362**, 2202-2211, doi:10.1056/NEJMra0804577 (2010).

2 Brodeur, G. M. Neuroblastoma: biological insights into a clinical enigma. *Nature reviews. Cancer* **3**, 203-216, doi:10.1038/nrc1014 (2003).

3 Ritenour, L. E., Randall, M. P., Bosse, K. R. & Diskin, S. J. Genetic susceptibility to neuroblastoma: current knowledge and future directions. *Cell and Tissue Research* **372**, 287-307, doi:10.1007/s00441-018-2820-3 (2018).

4 Cheung, N. K. & Dyer, M. A. Neuroblastoma: developmental biology, cancer genomics and immunotherapy. *Nature reviews. Cancer* **13**, 397-411, doi:10.1038/nrc3526 (2013).

5 Janoueix-Lerosey, I. *et al.* Overall genomic pattern is a predictor of outcome in neuroblastoma. *Journal of clinical oncology : official journal of the American Society of Clinical Oncology* **27**, 1026-1033, doi:10.1200/jco.2008.16.0630 (2009).

6 Peifer, M. *et al.* Telomerase activation by genomic rearrangements in high-risk neuroblastoma. *Nature* **526**, 700-704, doi:10.1038/nature14980 (2015).

7 Ackermann, S. *et al.* A mechanistic classification of clinical phenotypes in neuroblastoma. *Science (New York, N.Y.)* **362**, 1165-1170, doi:10.1126/science.aat6768 (2018).

8 Marshall, G. M. *et al.* The prenatal origins of cancer. *Nature reviews. Cancer* **14**, 277-289, doi:10.1038/nrc3679 (2014).

9 Le Douarin, N., LeDouarin, N. M. & Kalcheim, C. *The neural crest*. (Cambridge university press, 1999).

10 Ansieau, S., Morel, A. P., Hinkal, G., Bastid, J. & Puisieux, A. TWISTing an embryonic transcription factor into an oncoprotein. *Oncogene* **29**, 3173-3184, doi:10.1038/onc.2010.92 (2010).

11 Yeung, K. T. & Yang, J. Epithelial-mesenchymal transition in tumor metastasis. *Molecular oncology* **11**, 28-39, doi:10.1002/1878-0261.12017 (2017).

12 Franco, H. L., Casasnovas, J., Rodríguez-Medina, J. R. & Cadilla, C. L. Redundant or separate entities?--roles of Twist1 and Twist2 as molecular switches during gene transcription. *Nucleic acids research* **39**, 1177-1186, doi:10.1093/nar/gkq890 (2011).

13 el Ghouzzi, V. *et al.* Mutations of the TWIST gene in the Saethre-Chotzen syndrome. *Nature genetics* **15**, 42-46, doi:10.1038/ng0197-42 (1997).

14 Yang, J. *et al.* Twist, a master regulator of morphogenesis, plays an essential role in tumor metastasis. *Cell* **117**, 927-939, doi:10.1016/j.cell.2004.06.006 (2004).

15 Valsesia-Wittmann, S. *et al.* Oncogenic cooperation between H-Twist and N-Myc overrides failsafe programs in cancer cells. *Cancer cell* **6**, 625-630, doi:10.1016/j.ccr.2004.09.033 (2004).

16 Nozato, M., Kaneko, S., Nakagawara, A. & Komuro, H. Epithelial-mesenchymal transition-related gene expression as a new prognostic marker for neuroblastoma. *International journal of oncology* **42**, 134-140, doi:10.3892/ijo.2012.1684 (2013).

17 Selmi, A. *et al.* TWIST1 is a direct transcriptional target of MYCN and MYC in neuroblastoma. *Cancer letters* **357**, 412-418, doi:10.1016/j.canlet.2014.11.056 (2015).

18 Zeid, R. *et al.* Enhancer invasion shapes MYCN-dependent transcriptional amplification in neuroblastoma. *Nature genetics* **50**, 515-523, doi:10.1038/s41588-018-0044-9 (2018).

19 Zhang, W. *et al.* Comparison of RNA-seq and microarray-based models for clinical endpoint prediction. *Genome Biology* **16**, 133, doi:10.1186/s13059-015-0694-1 (2015).

20 Kocak, H. *et al.* Hox-C9 activates the intrinsic pathway of apoptosis and is associated with spontaneous regression in neuroblastoma. *Cell death & disease* **4**, e586, doi:10.1038/cddis.2013.84 (2013).

21 Eckert, M. A. *et al.* Twist1-induced invadopodia formation promotes tumor metastasis. *Cancer cell* **19**, 372-386, doi:10.1016/j.ccr.2011.01.036 (2011).

22 Balkwill, F. R., Capasso, M. & Hagemann, T. The tumor microenvironment at a glance. *Journal of cell science* **125**, 5591-5596, doi:10.1242/jcs.116392 (2012).

23 Sahai, E. *et al.* A framework for advancing our understanding of cancer-associated fibroblasts. *Nature Reviews Cancer* **20**, 174-186, doi:10.1038/s41568-019-0238-1 (2020).

24 Walker, G. A., Guerrero, I. A. & Leinwand, L. A. Myofibroblasts: molecular crossdressers. *Current topics in developmental biology* **51**, 91-107, doi:10.1016/s0070-2153(01)51003-0 (2001).

25 Mazzoccoli, G. *et al.* A primary tumor gene expression signature identifies a crucial role played by tumor stroma myofibroblasts in lymph node involvement in oral squamous cell carcinoma. *Oncotarget* **8**, 104913-104927, doi:10.18632/oncotarget.20645 (2017).

26 Baum, J. & Duffy, H. S. Fibroblasts and myofibroblasts: what are we talking about? *Journal of cardiovascular pharmacology* **57**, 376-379, doi:10.1097/FJC.0b013e3182116e39 (2011).

27 Tuxhorn, J. A. *et al.* Reactive stroma in human prostate cancer: induction of myofibroblast phenotype and extracellular matrix remodeling. *Clinical cancer research : an official journal of the American Association for Cancer Research* **8**, 2912-2923 (2002).

28 Georgoudaki, A. M. *et al.* Reprogramming Tumor-Associated Macrophages by Antibody Targeting Inhibits Cancer Progression and Metastasis. *Cell Rep* **15**, 2000-2011, doi:10.1016/j.celrep.2016.04.084 (2016).

29 Song, G. *et al.* Direct Reprogramming of Hepatic Myofibroblasts into Hepatocytes In Vivo Attenuates Liver Fibrosis. *Cell Stem Cell* **18**, 797-808, doi:10.1016/j.stem.2016.01.010 (2016).

30 Yeremenko, N. *et al.* Disease-specific and inflammation-independent stromal alterations in spondylarthritis synovitis. *Arthritis Rheum* **65**, 174-185, doi:10.1002/art.37704 (2013).

31 Ansieau, S. *et al.* Induction of EMT by twist proteins as a collateral effect of tumor-promoting inactivation of premature senescence. *Cancer cell* **14**, 79-89, doi:10.1016/j.ccr.2008.06.005 (2008).

32 Zhao, Z., Rahman, M. A., Chen, Z. G. & Shin, D. M. Multiple biological functions of Twist1 in various cancers. *Oncotarget* **8**, 20380-20393, doi:10.18632/oncotarget.14608 (2017).

33 Fang, X. *et al.* Twist2 contributes to breast cancer progression by promoting an epithelial-mesenchymal transition and cancer stem-like cell self-renewal. *Oncogene* **30**, 4707-4720, doi:10.1038/onc.2011.181 (2011).

34 Gasparotto, D. *et al.* Overexpression of TWIST2 correlates with poor prognosis in head and neck squamous cell carcinomas. *Oncotarget* **2**, 1165-1175, doi:10.18632/oncotarget.390 (2011).

35 Mao, Y., Xu, J., Song, G., Zhang, N. & Yin, H. Twist2 promotes ovarian cancer cell survival through activation of Akt. *Oncology letters* **6**, 169-174, doi:10.3892/ol.2013.1316 (2013).

36 Yu, H. *et al.* Twist2 is a valuable prognostic biomarker for colorectal cancer. *World journal of gastroenterology* **19**, 2404-2411, doi:10.3748/wjg.v19.i15.2404 (2013).

37 Beck, B. *et al.* Different levels of Twist1 regulate skin tumor initiation, stemness, and progression. *Cell Stem Cell* **16**, 67-79, doi:10.1016/j.stem.2014.12.002 (2015).

38 Shi, J. *et al.* Disrupting the interaction of BRD4 with diacetylated Twist suppresses tumorigenesis in basal-like breast cancer. *Cancer cell* **25**, 210-225, doi:10.1016/j.ccr.2014.01.028 (2014).

39 Mironchik, Y. *et al.* Twist overexpression induces in vivo angiogenesis and correlates with chromosomal instability in breast cancer. *Cancer research* **65**, 10801-10809, doi:10.1158/0008-5472.Can-05-0712 (2005).

40 Xu, Y. *et al.* Breast tumor cell-specific knockout of Twist1 inhibits cancer cell plasticity, dissemination, and lung metastasis in mice. *Proceedings of the National Academy of Sciences of the United States of America* **114**, 11494-11499, doi:10.1073/pnas.1618091114 (2017).

41 Fu, J. *et al.* The TWIST/Mi2/NuRD protein complex and its essential role in cancer metastasis. *Cell research* **21**, 275-289, doi:10.1038/cr.2010.118 (2011).

42 Bildsoe, H. *et al.* Transcriptional targets of TWIST1 in the cranial mesoderm regulate cell-matrix interactions and mesenchyme maintenance. *Developmental biology* **418**, 189-203, doi:10.1016/j.ydbio.2016.08.016 (2016).

43 Chen, Z. F. & Behringer, R. R. twist is required in head mesenchyme for cranial neural tube morphogenesis. *Genes & development* **9**, 686-699, doi:10.1101/gad.9.6.686 (1995).

44 Yochum, Z. A. *et al.* Targeting the EMT transcription factor TWIST1 overcomes resistance to EGFR inhibitors in EGFR-mutant non-small-cell lung cancer. *Oncogene* **38**, 656-670, doi:10.1038/s41388-018-0482-y (2019).

45 Martin, A. & Cano, A. Tumorigenesis: Twist1 links EMT to self-renewal. *Nature cell biology* **12**, 924-925, doi:10.1038/ncb1010-924 (2010).

46 Schmidt, J. M. *et al.* Stem-cell-like properties and epithelial plasticity arise as stable traits after transient Twist1 activation. *Cell Rep* **10**, 131-139, doi:10.1016/j.celrep.2014.12.032 (2015).

47 Mani, S. A. *et al.* The epithelial-mesenchymal transition generates cells with properties of stem cells. *Cell* **133**, 704-715, doi:10.1016/j.cell.2008.03.027 (2008).

48 Coulon, A. *et al.* Functional sphere profiling reveals the complexity of neuroblastoma tumor-initiating cell model. *Neoplasia* **13**, 991-1004, doi:10.1593/neo.11800 (2011).

49 Winkler, J., Abisoye-Ogunniyan, A., Metcalf, K. J. & Werb, Z. Concepts of extracellular matrix remodelling in tumour progression and metastasis. *Nature communications* **11**, 5120, doi:10.1038/s41467-020-18794-x (2020).

50 Tadeo, I. *et al.* Extracellular matrix composition defines an ultra-high-risk group of neuroblastoma within the high-risk patient cohort. *British journal of cancer* **115**, 480-489, doi:10.1038/bjc.2016.210 (2016).

51 Chakraborty, S. *et al.* Twist1 promotes heart valve cell proliferation and extracellular matrix gene expression during development in vivo and is expressed in human diseased aortic valves. *Developmental biology* **347**, 167-179, doi:10.1016/j.ydbio.2010.08.021 (2010).

52 García-Palmero, I. *et al.* Twist1-induced activation of human fibroblasts promotes matrix stiffness by upregulating palladin and collagen α1(VI). *Oncogene* **35**, 5224-5236, doi:10.1038/onc.2016.57 (2016).

53 Shamir, E. R., Coutinho, K., Georgess, D., Auer, M. & Ewald, A. J. Twist1-positive epithelial cells retain adhesive and proliferative capacity throughout dissemination. *Biology open* **5**, 1216-1228, doi:10.1242/bio.019703 (2016).

54 Wang, S. *et al.* Up-regulation of PCOLCE by TWIST1 promotes metastasis in Osteosarcoma. *Theranostics* **9**, 4342-4353, doi:10.7150/thno.34090 (2019).

55 Puissant, A. *et al.* Targeting MYCN in neuroblastoma by BET bromodomain inhibition. *Cancer Discov* **3**, 308-323, doi:10.1158/2159-8290.CD-12-0418 (2013).

56 Dubois, S. G. *et al.* Lung metastases in neuroblastoma at initial diagnosis: A report from the International Neuroblastoma Risk Group (INRG) project. *Pediatric blood & cancer* **51**, 589-592, doi:10.1002/pbc.21684 (2008).

57 Chen, Q., Wang, J., Liu, W. N. & Zhao, Y. Cancer Immunotherapies and Humanized Mouse Drug Testing Platforms. *Transl Oncol* **12**, 987-995, doi:10.1016/j.tranon.2019.04.020 (2019).

58 Seeger, R. C. *et al.* Morphology, growth, chromosomal pattern and fibrinolytic activity of two new human neuroblastoma cell lines. *Cancer research* **37**, 1364-1371 (1977).

59 Biedler, J. L. & Spengler, B. A. A novel chromosome abnormality in human neuroblastoma and antifolate-resistant Chinese hamster cell lives in culture. *J Natl Cancer Inst* **57**, 683-695, doi:10.1093/jnci/57.3.683 (1976).

60 Shalem, O. *et al.* Genome-scale CRISPR-Cas9 knockout screening in human cells. *Science (New York, N.Y.)* **343**, 84-87, doi:10.1126/science.1247005 (2014).

61 Sanjana, N. E., Shalem, O. & Zhang, F. Improved vectors and genome-wide libraries for CRISPR screening. *Nature methods* **11**, 783-784, doi:10.1038/nmeth.3047 (2014).
62 Flahaut, M. *et al.* Aldehyde dehydrogenase activity plays a Key role in the aggressive phenotype of neuroblastoma. *BMC Cancer* **16**, 781, doi:10.1186/s12885-016-2820-1 (2016).
63 Carr, J. *et al.* High-resolution analysis of allelic imbalance in neuroblastoma cell lines by single nucleotide polymorphism arrays. *Cancer genetics and cytogenetics* **172**, 127-138, doi:10.1016/j.cancergencyto.2006.08.012 (2007).
64 Joseph, J. M. *et al.* In vivo echographic evidence of tumoral vascularization and microenvironment interactions in metastatic orthotopic human neuroblastoma xenografts. *Int J Cancer* **113**, 881-890, doi:10.1002/ijc.20681 (2005).
65 Kulak, N. A., Pichler, G., Paron, I., Nagaraj, N. & Mann, M. Minimal, encapsulated proteomic-sample processing applied to copy-number estimation in eukaryotic cells. *Nature methods* **11**, 319-324, doi:10.1038/nmeth.2834 (2014).
66 Cox, J. & Mann, M. MaxQuant enables high peptide identification rates, individualized p.p.b.-range mass accuracies and proteome-wide protein quantification. *Nature biotechnology* **26**, 1367-1372, doi:10.1038/nbt.1511 (2008).
67 Cox, J. *et al.* Andromeda: a peptide search engine integrated into the MaxQuant environment. *Journal of proteome research* **10**, 1794-1805, doi:10.1021/pr101065j (2011).
68 Schwanhäusser, B. *et al.* Global quantification of mammalian gene expression control. *Nature* **473**, 337-342, doi:10.1038/nature10098 (2011).
69 Cox, J. *et al.* Accurate proteome-wide label-free quantification by delayed normalization and maximal peptide ratio extraction, termed MaxLFQ. *Molecular & cellular proteomics : MCP* **13**, 2513-2526, doi:10.1074/mcp.M113.031591 (2014).
70 Tyanova, S. *et al.* The Perseus computational platform for comprehensive analysis of (prote)omics data. *Nature methods* **13**, 731-740, doi:10.1038/nmeth.3901 (2016).

Acknowledgements

We thank Dr. Manfredo Quadroni (Protein Analysis Facility, University of Lausanne) and his team for their help with the secretome analysis. Dr Jessica Dessimoz (Histology Core Facility of the EPFL) and Janine Horlbeck (Mouse Pathology Facility) for their help with the IHC and tissue staining. Dr Julien Marquis (Lausanne Genomics Technologies Facility) for his technical advice in the targeted sequencing analysis of the indels in TWIST1 gene. This work was supported by grants from Kinderkrebsforschung Schweiz (to A.M.M.), the Novartis Foundation for Medical-Biological Research (to A.M.M.), the Hubert Gouin Association (to A.M.M.), and the FORCE foundation (to A.M.M. and R.R.).

Author contributions

M.V.S. performed all major experimental work, with the technical help of K.B.B., M.V.S. and A.M.M. analyzed the data, prepared figures and drafted the manuscript, J.M.J and N.J. performed *in vivo* xenograft implantations, K.N.A. constructed the LentiCRISPR v2-sgTWIST1 vectors, J.Y.S. provided the TMA., H.S. performed the TMA analysis and the interpretation of the related data, A.P. provided help in the TMA analysis, V.P. conducted the bioinformatics analysis, N.R. performed pathological analyses of the xenografts, R.R. interpreted the data

and edited the manuscript, A.M.M. designed, supervised the study and coordinated experiments. All authors read, commented and approved the final manuscript.

Competing interests

The authors declare no competing interests.

Correspondence and requests for materials should be addressed to A.M.M.

Figures and Figure Legends

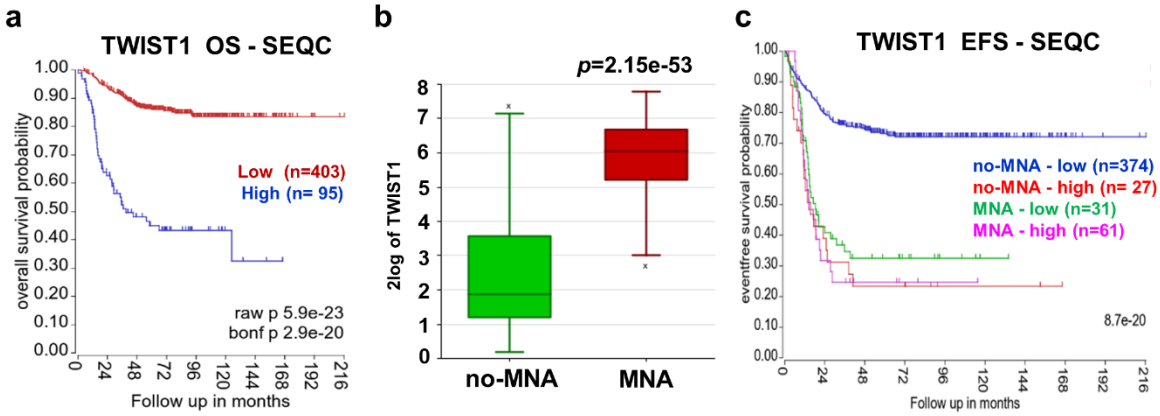

Figure 1. TWIST1 RNA expression is associated with poorer outcome of NB patients. (**a-c**) Analysis of TWIST1 expression in the SEQC dataset of primary NB tumors. (**a**) Kaplan-Meier OS curve associated with TWIST1 expression. Expression cutoff: 44.441. (**b**) Box-and-whisker plots of TWIST1 expression in tumors with MNA or without MNA (no-MNA). (**c**) Kaplan-Meier EFS curves showing the stratification of patients according to MYCN status and TWIST1 expression (high or low).

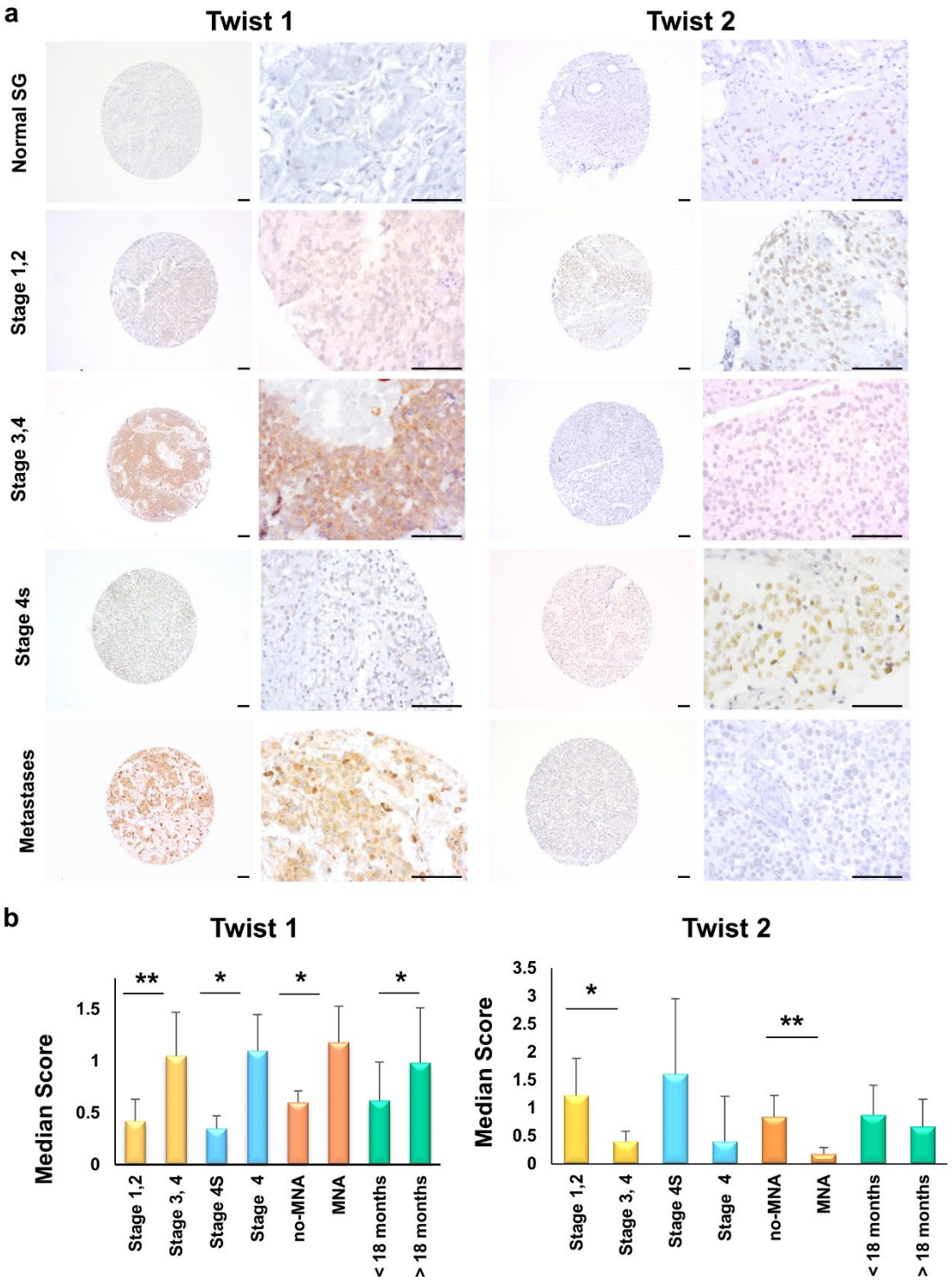

941

942

943 **Figure 2. TWIST1 and TWIST2 display an opposite protein expression profile in a NB**
944 **tissue microarray.** (**a**) TWIST1 and TWIST2 protein expression were analyzed by IHC using
945 a NB TMA containing 97 tumor sections: 72 primary tumors, 25 matched metastases and 44
946 matched control normal tissues (i.e. SG). Representative images of TWIST1 and TWIST2 IHC

947 staining are shown for each indicated category. Magnification 100x (left panels) and 400x (right
948 panels); scale bares=100 μm. (**b**) Bar graphs showing the median scores (ms) ± SD of TWIST1
949 and TWIST2 IHC staining for different comparisons (see Table 1). Statistical analysis was done
950 using parametric Student's t-test.

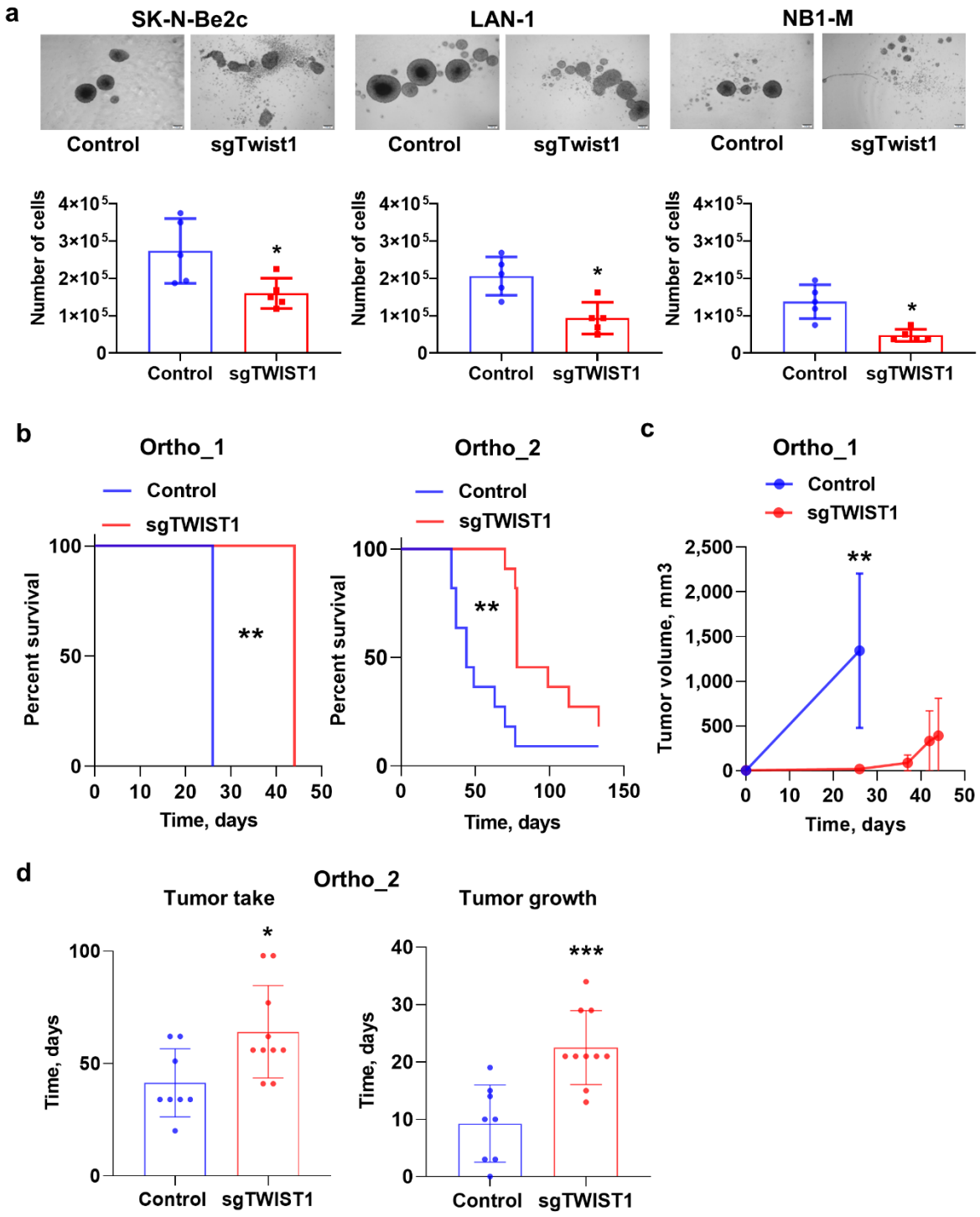

Figure 3. TWIST1 KO reduces the neurosphere forming capacities of NB cells *in vitro* and the tumor growth capacities of SK-N-Be2c cells *in vivo*. (**a**) Upper panel: representative images (scale bar 200 µm) showing the size and shape of primary neurospheres of Control and sgTWIST1 NB cells after 7 days in culture. Lower panel: the numbers of cells obtained after dissociation of Control and sgTWIST1 primary neurospheres are plotted in bare graphs as individual values for each independent experiments and mean ± SD (n=5 experiments performed in duplicates). Mann Whitney test: *p=0.0317 for SK-N-Be2c;

*p=0.0159 for LAN-1 and NB1-M. (**b**) Kaplan-Meier survival curves of athymic Swiss nude mice implanted with SK-N-Be2C-Control or -sgTWIST1 cells. Mice were sacrificed once tumors reached the volume of 1000 mm^3 and 500 mm^3 for ortho_1 and ortho_2 experiments, respectively. Tumor take: ortho_1: 100% (6/6) in the Control group, 66.66% (4/6) in the sgTWIST1 group; ortho_2: 89% (8/9) in the Control group, 83% (10/12) in the sgTWIST1 group. Median survival in the Control vs sgTWIST1 group: 26 vs 44 days for ortho_1 (**p=0.0027); 49 vs 78 days for ortho_2 (**p=0.0016). Gehan-Breslow-Wilcoxon test. (**c**)Tumor growth (mean tumor volumes ± SD) for ortho_1 experiment. Multiple t-test (Holm-Sidak, α=0.05, without assuming a consistent SD): **p=0.0037. (**d**) Time for tumor initiation (left) and tumor growth (right) in the ortho_2 experiment (mean days ± SD). Tumor initiation correspond to the number of days required to measure an AG volume > 10 mm^3 (mean Control: 41.38 days, sgTWIST1: 64.10 days, *p=0.0192). Time for tumor growth was calculated as the number of days at sacrifice minus the number of days for tumor initiation (mean Control: 9.25 days, sgTWIST1: 22.50 days, ***p=0.0006). Unpaired t-test.

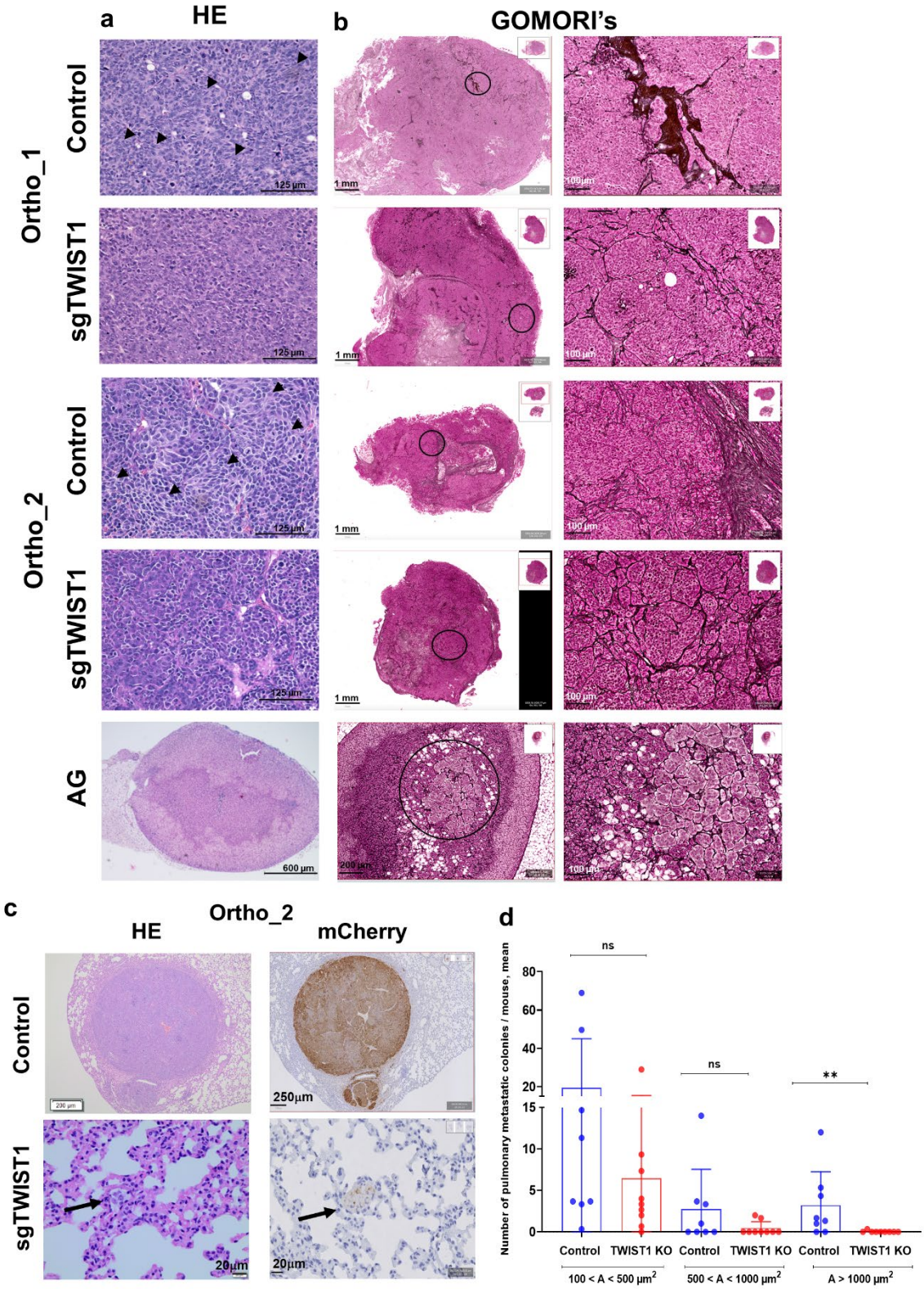

Figure 4. TWIST1 KO produces tumor with a less aggressive phenotype and impairs the formation of the intrapulmonary macrometastases. (**a**) Representative images of H&E staining of ortho tumors and AG. H&E staining of both ortho-derived tumors depicted cells in

977 control tissues separated by thin fibro-vascular septs having irregular size and shape; no
978 discernable/scarce cytoplasm; one or few prominent nucleoli; spindle-shaped cells with
979 fusiform nuclei (black arrow) that tended to have a fascicular organization. Conversely,
980 sgTWIST1 tumor cells were portrayed by a more regular size and shape (round to oval) with
981 only slight irregularities, finely granular ("salt-and-pepper") chromatin, small nucleoli and
982 moderate/more discernible cytoplasm (scale bar: 125 µm for tumors; 600µm for AG). (**b**)
983 Representative images of Gomori's staining showing the architecture of the collagen
984 III/reticulin fibers in ortho tumors and AG. Left panels: large views of tumor and AG sections;
985 scale bars: 1 mm and 200 µm, respectively. Right panels: zoomed view of the region
986 highlighted by a black circle, scale bars: 100 µm for both tumors and AG. (**c**) H&E and anti-
987 mCherry staining for pulmonary metastases detection in the lungs of ortho_2 mice. Upper
988 panel: representative images of Control mice; lower panel: pictures of the unique
989 macrometastasis detected in sgTWIST1 group of mice. (**d**) Quantification of metastases
990 detected by IHC anti-mCherry within the parenchyma (intrapulmonary) of mice. Of note, no
991 metastases were detected at the pleural surface and/or in mediastinal soft tissue
992 (peripulmonary). Data are plotted in a bar graph showing individual values and mean ± SD for
993 micrometastases (100-500 μm^2: p=0.2257; 500-1000 μm^2: p=0.1855) and for
994 macrometastases (>1000 μm^2, **p= 0.0041). Mann-Whitney test. Percent of mice with
995 macrometastases = 75% in the Control group; 10% in the sgTWIST1 group.

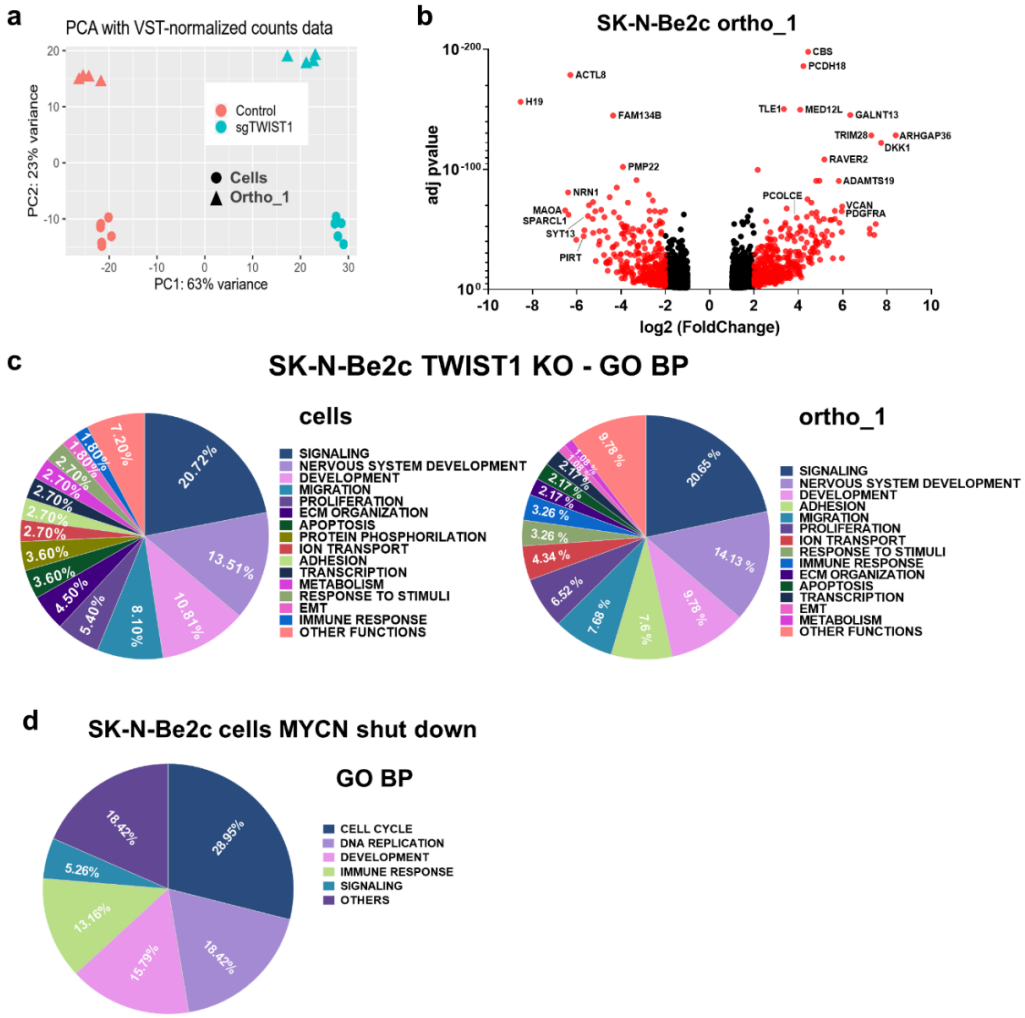

Figure 5. The biological pathways deregulated by TWIST1 KO are distinct from those mediated by MYCN shut down. (**a**) PCA samples repartition using the VST-normalized counts. PCA1 and PCA2 are 63% and 23% of total variation, respectively. (**b**) Volcano plots showing the distribution of the DE genes according to FC (log2) and adj *p* value between the SK-N-Be2c-Control and –sgTWIST1 ortho_1-derived xenografts. Genes with False Discovery Rate (FDR) < 0.05 and absolute value (av) of log2(FC) ≥ 1 were considered as DE; in red genes with av of log2(FC) ≥2, in black genes with av of log2(FC) ≥ 1 and <2. Positive and negative x-values represent genes either up- or down-regulated by TWIST1, respectively. (**c**)**.** Illustration of the biological processes gene sets found enriched by GO analyses (GO BP) in the DE genes following TWIST1 KO for both SK-N-Be2c cells (left panel) and ortho_1 tumors (right panel). Data are reported as the repartition (in %) of the diverse pathways identified with a FDR < 0.01 (n=111 for cells, n=92 for tumors). (**d**) Illustration of the GO BP gene sets found enriched in the DE genes in SK-N-Be2c cells upon JC1-medited MYCN shutdown. RNAseq data of SK-N-Be2c cells treated with JC1 during 24h or DMSO as control were uploaded (GSE80154, see Methods) (Zeid et al.). Genes with False Discovery Rate (FDR) < 0.05 and

absolute value (av) of log2(FC) ≥ 1 were considered as DE. Data are reported as the repartition (in %) of the diverse pathways identified with a FDR < 0.01 (n=38).

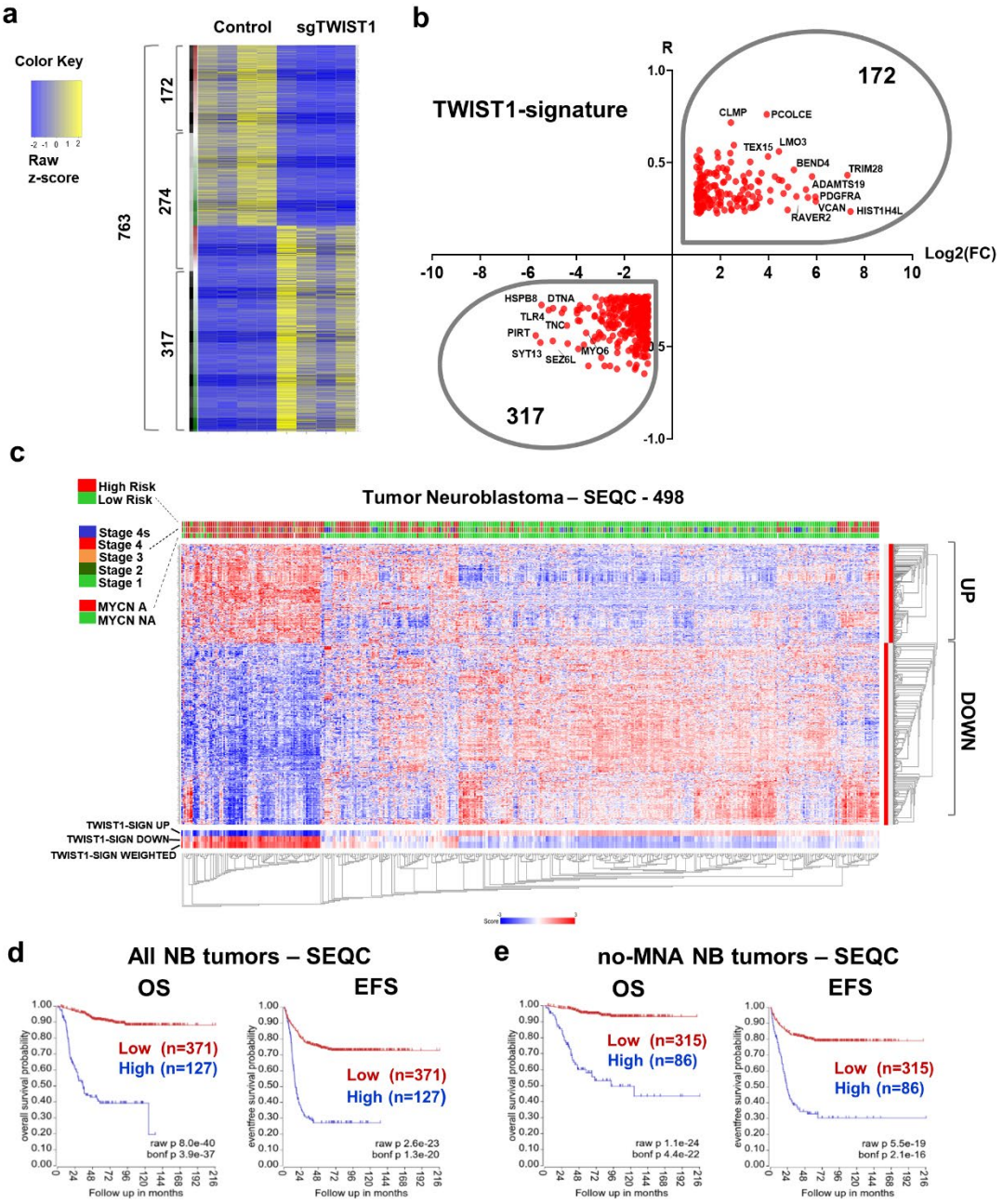

Figure 6. **Identification of a TWIST1-associated gene signature correlating with poor prognosis in NB**. (**a**) Heatmap showing 763 common genes either correlated or anti-correlated with TWIST1 in NB patients and DE in the ortho_1 tumors. The binary side color bar going from green to red indicates DE genes anti-correlated (R<-0.225, green) or correlated (R>0.225, red) with TWIST1 in the SEQC dataset; the black bar shows the genes that have both FC and R values either positive or negative representing the TWIST1-signature, and the grey bar the genes that have opposite FC and R values (not included in the signature). (**b**) Volcano plot showing the distribution of the 489 genes of the TWIST1-signature according to their log2(FC) in SK-N-Be2c ortho_1 tumors and R values in the SEQC dataset . (**c**) Heatmap

hierarchical clustering showing different expression pattern relative to TWIST1-signature genes generated using the R2 Platform (http://r2.amc.nl). Columns represent patients annotated in the SEQC cohort; the 489 genes are clustered hierarchically along the left y-axis. Clinical criteria taken into consideration (risk groups, tumor stages, and MYCN amplification status) are indicated on the top by color codes. The heat map indicates in red, blue and white a high, low and a medium level of gene expression (z-score), respectively. The blue-white-red color bars depicted at the bottom of the heatmap represent the z-score of TWIST1_Up and TWIST1_Down gene sub-lists of the signature, as well as for the z-score of the whole signature (weighted). (**f-g**) Kaplan-Meier OS and EFS survival curves according to the expression level of the TWIST1-signature in both the complete SEQC dataset (**f**) and in the sub-cohort of patients without MNA (no-MNA) (**g**). Expression cutoff: 0.20 (**f**) and -0.05 (**g**).

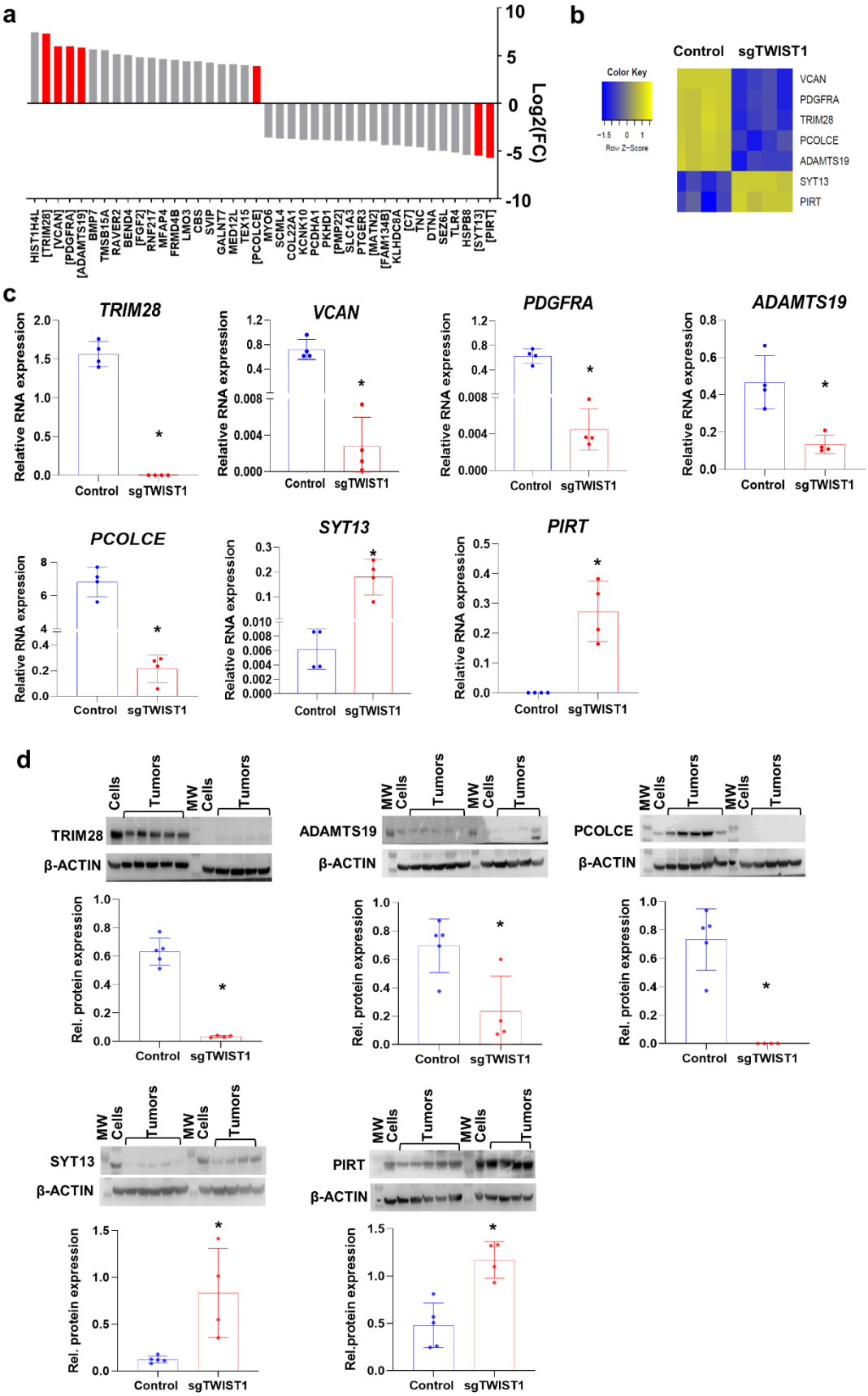

Figure 7. Validation of TWIST1-mediated deregulation of selected genes belonging to the TWIST1 signature in the ortho_1 tumors. (**a**) Bar plots showing the distribution of the top 20 up- and 20 down-regulated genes of the TWIST1 signature ordered according to their log2(FC). In red, genes that were selected for the validation at both RNA and protein levels. Gene names in brackets indicate up-regulated genes involved in the EMT process, TME organization, proliferation and apoptosis; and down-regulated genes that are known to be tumor suppressor genes or associated with good prognosis in NB. (**b**) Heatmap showing the relative RNA expression (z-score) determined by RNAseq of the selected genes in ortho_1 tumors. (**c**) RNA expression levels of the TWIST1 target genes relative to the reference gene *HPRT1* in the ortho_1 tumors analyzed by RT-qPCR are plotted as individual values with mean ± SD. Control n= 6 ; sgTWIST1 n= 4. Mann Whitney test: **p*=0.0286 for all comparisons. (**d**) Upper panel: Immunoblotting for TRIM28, ADAMTS19, PCOLCE, ADAMTS19, SYT13 and PIRT (β-ACTIN as the loading control); lower panel: densitometric quantifications of immunoreactive band densities. Expression relative to β-ACTIN were plotted as individual data with mean ± SD. Control n= 5; sgTWIST1n= 4 . Mann Whitney test: **p*= 0.0317 for ADAMTS19; **p*= 0.0159 for the other proteins.

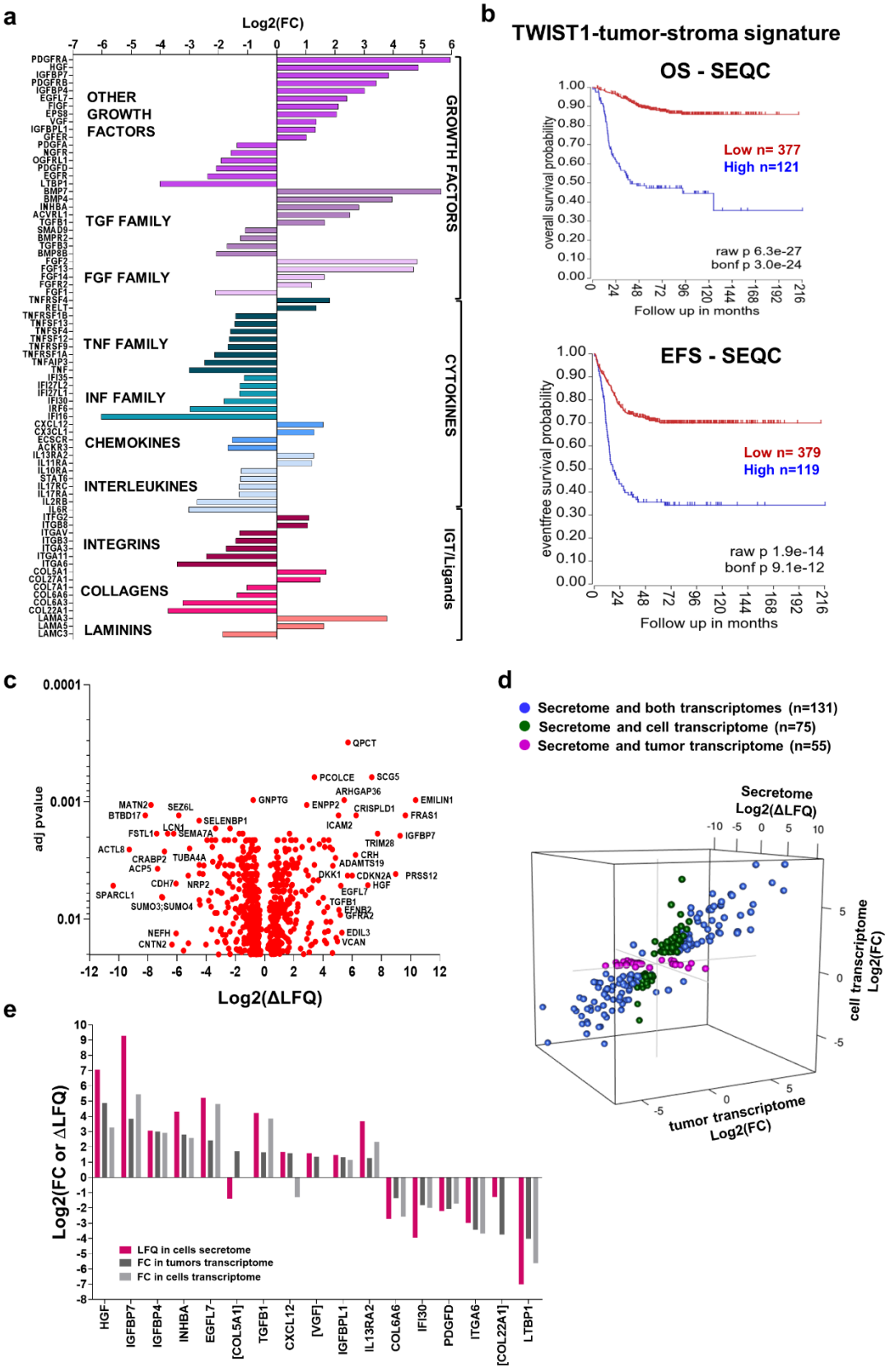

Figure 8. **Identification of a TWIST1-mediated-tumor-stroma signature associated with poor outcome in NB.** (**a**) Bar plot illustrating of the 77 DE genes representing the TWIST1-

tumor-stroma signature in SK-N-Be2c ortho_1 tumors. Genes were classified according to their log2(FC) in three main categories: growth factors (including the TGF and FGF families). cytokines (TNF and INF families, chemokines and interleukins), and integrins and their ligands (ITG, collagens and laminins). (**b**) Kaplan-Meier OS and EFS curves of NB patients of the SEQC dataset according to the expression level of the TWIST1-tumor-stroma signature. Expression cutoff for both curves: 0.10. (**c**) Volcano plot showing the distribution of the DE protein secreted by SK-N-Be2c cells according to the delta label-free quantification (ΔLFQ = LFQ SK-N-Be2c Control – LFQ SK-N-Be2c sgTWIST1) intensities (Log2) and the adjusted *p* values with an FDR ≤ 0.02 analyzed by LC-MS/MS (n= 3 biological replicates for each group). (**d**) 3D scatterplot showing DE terms in the cell secretome in common with the tumor transcriptome (magenta, n=55), the cell transcriptome (green, n=75), or both transcriptomes (blue, n=131). (**e**) Bar plot showing the terms commonly deregulated between the TWIST1-tumor-stroma signature and both the cell transcriptome and secretome. Names in brackets are for terms found to be DE in the secretome but not in the transcriptome of cells.

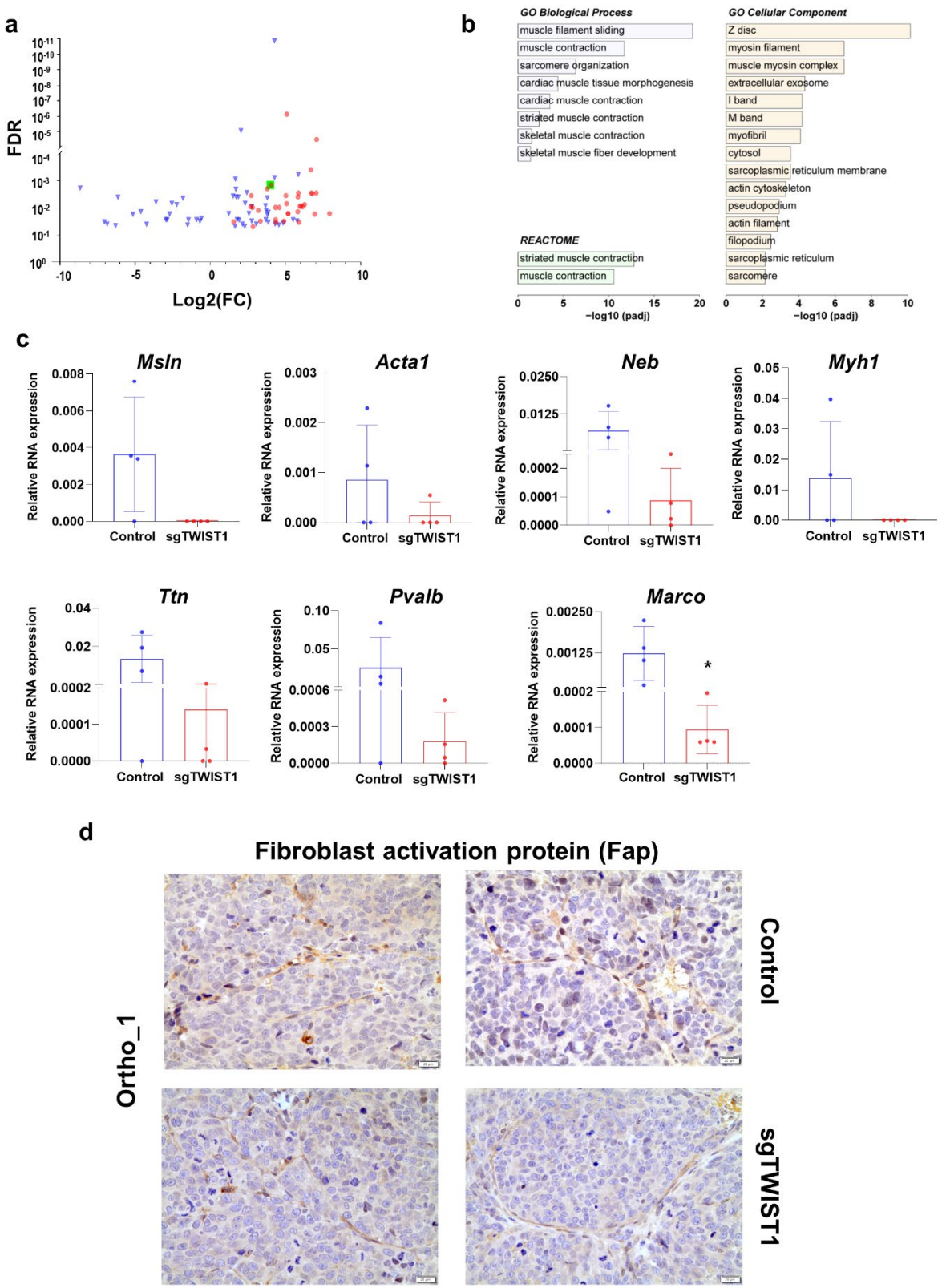

Figure 9. **Identification of a TWIST1-associated myofibroblast signature**. (**a**) Volcano plots showing the distribution of the DE gene identified in SK-N-Be2c-Control and –sgTWIST1 tumor stroma of ortho_1 xenografts relative to their log2(FC) and adjusted *p* value (FDR). Genes with FDR < 0.05 and absolute value (av) of log2(FC) ≥ 0.5 were considered as DE. Genes identified

as the Myofibroblast signature are indicated in red (n=36). The green square is for the gene *Marco*. (**b**) Bar graph showing the biological processes, cellular components and REACTOME pathways identified by GO analysis of the 89 DE genes of the murine stroma, listed according to their adjusted *p* value. (**c**) mRNA expression levels of the selected myofibroblast genes and Marco relative to β-actin as by RT-qPCR. Data are plotted as individual values with mean ± SD. Mann Whitney test: **p*= 0.0286. Ortho_1 Control and sgTWIST1 tumors: n=4. (**d**) IHC for the cancer-associated fibroblast marker Fibroblasts Activation Protein (FAP) on ortho_1 Control and sgTWIST1 tumors. Representative images of FAP positive cells characterized by spindle or fusiform morphologies and haphazardly arranged are shown (400x, scale bar: 20 μm).

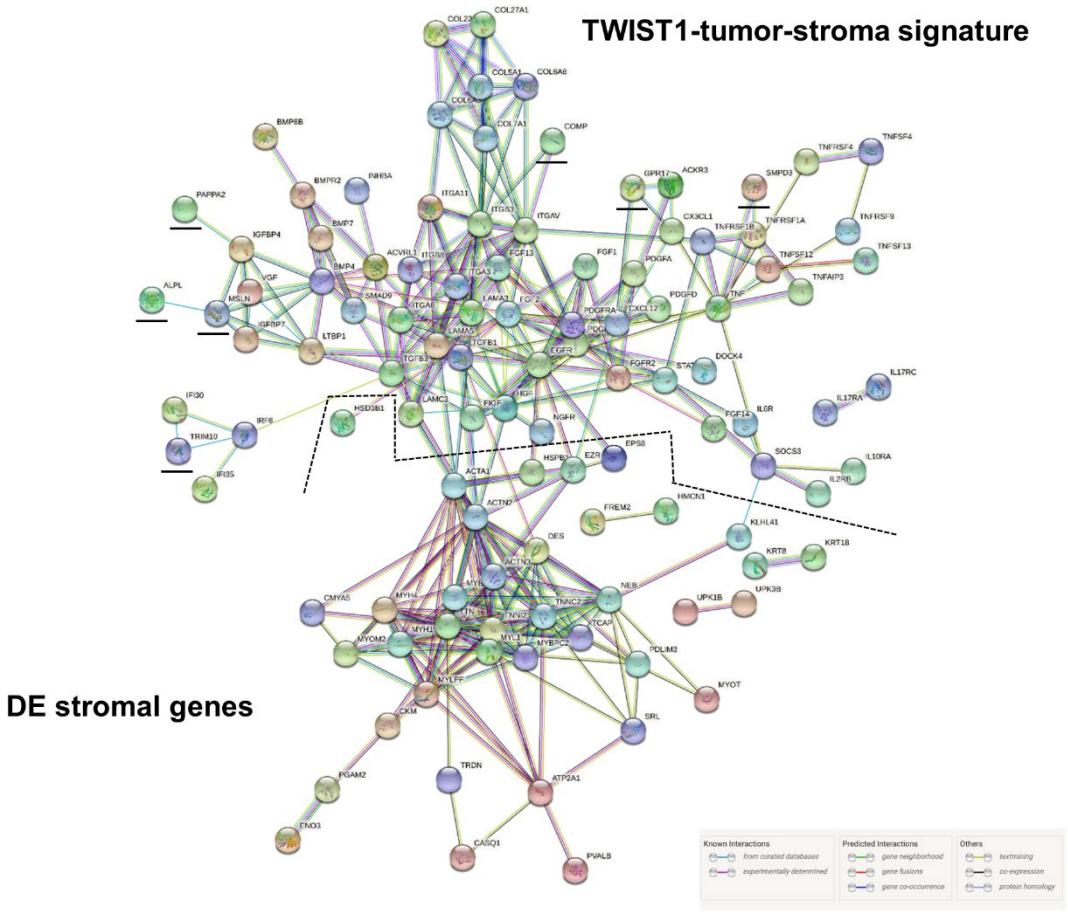

Figure 10. **PPI network for the TWIST1-associated tumor-stroma signature and the DE stromal genes.** Analysis of the protein-protein interactions between the TWIST1-tumor-stroma signature (n= 77 genes) and the DE murine stromal genes (n=89)**.** Direct (physical) as well as indirect (functional) interactions analyzed using the String website. All the basic and advanced default settings have been kept but the minimum required interaction score, that has been changed in high confidence (0.7); and the network display options, hiding the disconnected nodes in the network. PPI enrichment *p* value: $<1.0^{e}$-16. Murine stromal genes clustering with the TWIST1 tumor-stroma signature are underlined in black.

	Total n (%)	TWIST1				TWIST2			
		Positive tissue n (%)	Median score	SD	*p* value	Positive tissue n (%)	Median score	SD	*p* value
Sample Type									
Primary tumor	72	52 (72)	0.84	0.78		30 (42)	1.1	0.87	
Metastasis	25	19 (76)	0.95	0.74		8 (32)	0.31	0.3	
Lymph node	22	18 (82)	1.05	0.72		7 (32)	0.3	0.53	
Liver	3	1 (33)	0.66	0.31		1 (33)	0.75	0.35	
Control normal tissu = SG	44	0 (0)	0	0		20 (45)	0.58	0.53	
Age (mo)									
Median (range)									
<18 months	27	8 (30)	0.62	0.37	*p=0.045	16 (59)	0.87	0.53	ns
≥ 18 months	45	33 (73)	0.98	0.53		26 (58)	0.66	0.49	
INSS stage									
1	12 (16.7)	4 (33)	0.41	0.19		4 (33)	1.08	0.98	
2	6 (8.3)	3 (50)	0.41	0.24		3 (50)	1.5	0.52	
3	13 (13.8)	10 (77)	1.03	0.48		7 (54)	0.37	0.2	
4	36 (50)	30 (83)	1.1	0.35	*p=0.04	13 (36)	0.4	0.18	ns
4S	5 (6.9)	2 (40)	0.35	0.12		3 (60)	1.6	1.35	
1, 2	18 (25)	7 (39)	0.42	0.21	**p<0.01	7 (39)	1.22	0.67	*p=0.045
3, 4	49 (68)	40 (82)	1.05	0.42		20 (41)	0.4	0.18	
MYCN amplification									
MNA	13	11 (85)	1.18	0.35	*p=0.02	3 (23)	0.17	0.12	**p<0.01
no-MNA	47	11 (23)	0.6	0.11		22 (47)	0.84	0.38	

Table 1. Composition of the TMA and expression of TWIST1 and TWIST2 in NB primary tumors, metastases and control tissues. SG: sympathetic ganglia, INSS: International Neuroblastoma Staging System, n: number of cases. Median score means average tumor score, as established by semi-quantitative analysis of the immunostaining. Student's t-test: *p<0.05, **p<0.01, p≥0.05 were considered as not significant (ns).

Gene description	Gene	log2FC	padj	
Desmin	Des	1.5436	0.0326	Myofibroblast markers
Mesothelin	Msln	5.0785	7.2658E-07	
Actin, alpha 1, skeletal muscle	Acta1	6.6873	0.0004	Sarcomeric thin filament
Actinin alpha 2	Actn2	5.0222	0.0035	
Actinin alpha 3	Actn3	5.8876	0.0337	
Myosin binding protein C, slow-type	Mybpc1	6.7193	0.0028	
Nebulin	Neb	4.8947	0.0307	
Nebulin-related anchoring protein	Nrap	7.0611	3.0668E-05	
Troponin C2, fast	Tnnc2	6.9370	0.0169	
Troponin I, skeletal, fast 2	Tnni2	5.0686	0.0069	
Xin actin-binding repeat containing 2	Xirp2	5.1731	0.0162	
Cardiomyopathy associated 5	Cmya5	3.8505	0.0337	Sarcomeric thick filament
Myosin binding protein C, fast-type	Mybpc2	5.9514	0.0087	
Myosin, heavy polypeptide 1, skeletal muscle, adult	Myh1	6.0248	0.0084	
Myosin, heavy polypeptide 4, skeletal muscle, adult	Myh4	6.7812	0.0029	
Myosin, light polypeptide 1	Myl1	5.8567	0.0028	
Myosin light chain, phosphorylatable, fast skeletal muscle	Mylpf	6.2615	0.0075	
Myomesin 2	Myom2	4.3271	0.0096	
Myotilin	Myot	4.3341	0.0273	
Myelin regulatory factor	Myrf	2.7196	0.0035	
Titin-cap	Tcap	5.8251	0.0039	
Titin	Ttn	5.1708	0.0161	
Parvalbumin	Pvalb	7.9325	0.1618	Calcium ion-binding protein

Table 2. Summary of myofibroblast markers and principal muscle structure-specific genes identified in the myofibroblast signature of ortho_1 tumors (labeled in red in **Fig. 9a)** with their log2(FC) and adjusted *p* values.

Supplementary Figure 1

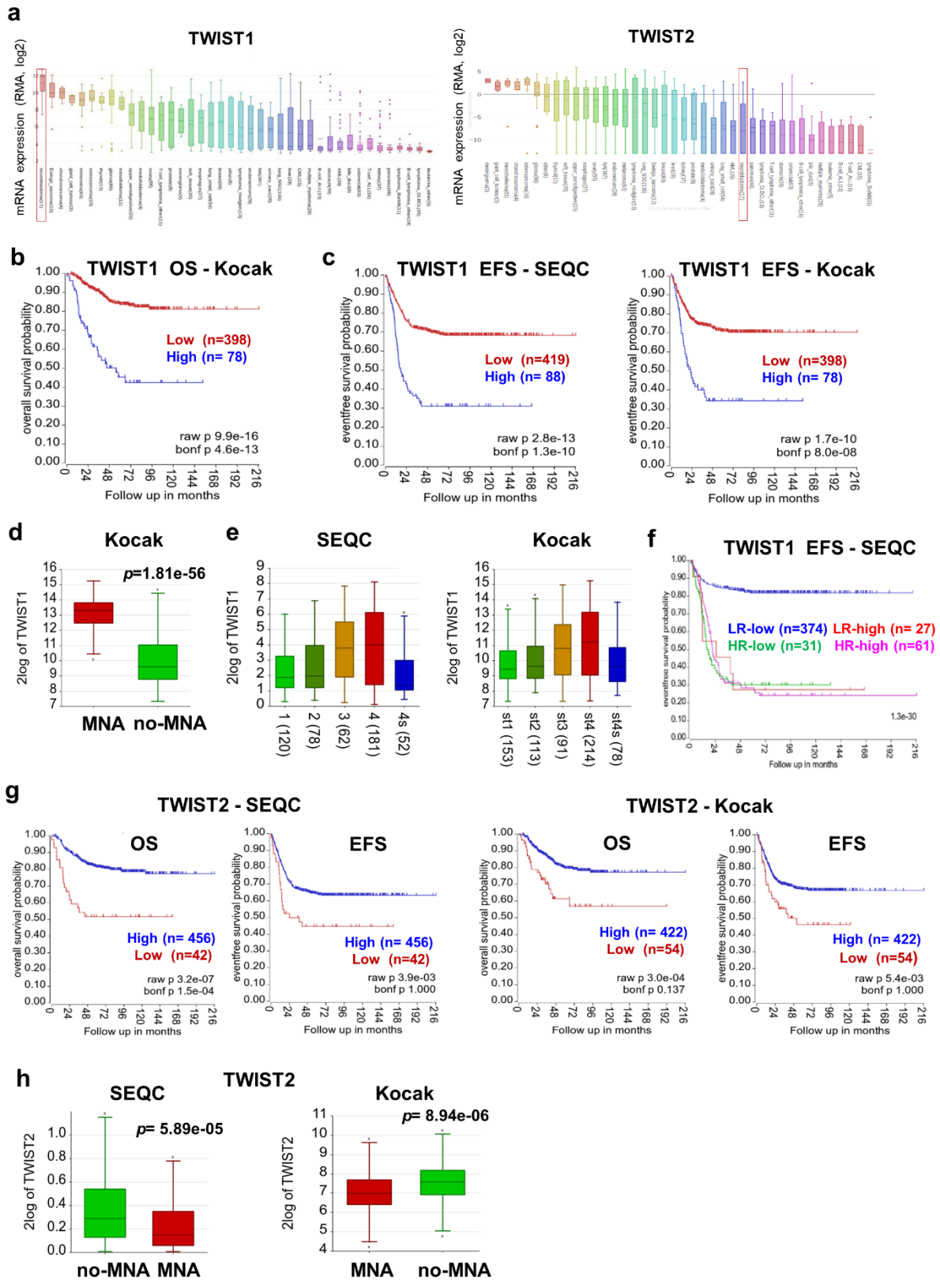

Supplementary Fig. 1. **TWIST1 and TWITS2 RNA expression in NB cells and tumors**. (**a**) Box plot showing the mRNA expression levels of TWIST1 (left) and TWIST2 (right) in a panel of 40 cancer cell lines in the CCLE database. The numbers in the brackets correspond to the numbers of cell lines per tumor types. (**b**) Kaplan-Meier OS curve associated with TWIST1 expression in the Kocak dataset of primary NB tumors (expression cutoff = 6701.9) (n=476 with survival data). (**c**) EFS associated with TWIST1 expression in the SEQC (left panel, expression cutoff: 44.441) and Kocak (right panel, expression cutoff = 6701.9) datasets. (**d-e**) Box-and-whisker plots of TWIST1 expression in MNA and no-MNA tumors (**d**); and in tumors with distinct INSS stages in the indicated datasets (**e**). (**f**) Kaplan-Meier EFS curves showing the stratification of patients of the SEQC dataset according to the risk classification (high-risk: HR; low-risk: LR) and TWIST1 expression (high or low). (**g**) OS and EFS according to TWIST2 expression in the SEQC (left panels, expression cutoff: 1010) and Kocak (right panels, expression cutoff: 86.0) datasets. (**h**) Box-and-whisker plots of TWIST2 expression in no-MNA and MNA tumors in the SEQC and Kocak datasets.

Supplementary Figure 2

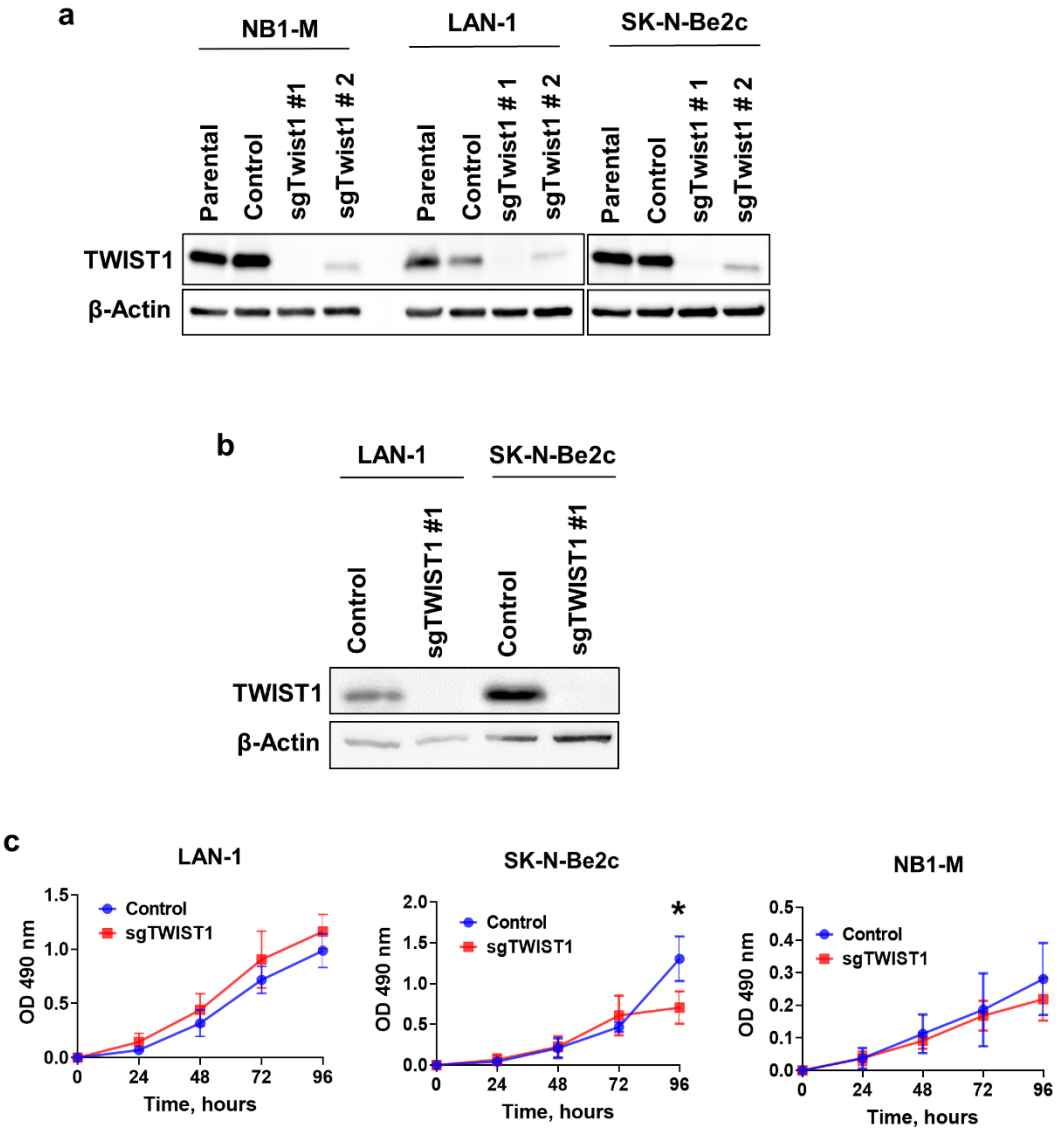

Supplementary Fig. 2. Validation of the CRISPR/Cas9-mediated TWIST1 KO and its impact on NB cell proliferation *in vitro*. (**a**) Immunoblotting for the detection of TWIST1 protein expression and β-actin (as the loading control) in the bulk populations of NB cells before (Parental) and after the lentiviral infection: Control vector, sgTWIST1#1 (sgTWIST1, from now on) and sgTWIST1#2. (**b**) TWIST1 protein expression in the LAN-1 and SK-N-Be2c pool of clones for Control and sgTWST1 (see Matherial&Methods). (**c**) Cell proliferation of Control and sgTWST1 NB cell lines measured by MTS/PMS assay from 24h to 96h. Mean OD 490nm ± SD of three (SK-N-Be2c) and four (LAN-1 and NB1-M) independent experiments performed in quadruplicates are shown. Statistical analysis was done using the Holm-Sidak multiple t-test (α=0.05), without assuming a consistent SD. *p= 0.0376 in SK-N-Be2c.

Supplementary Figure 3

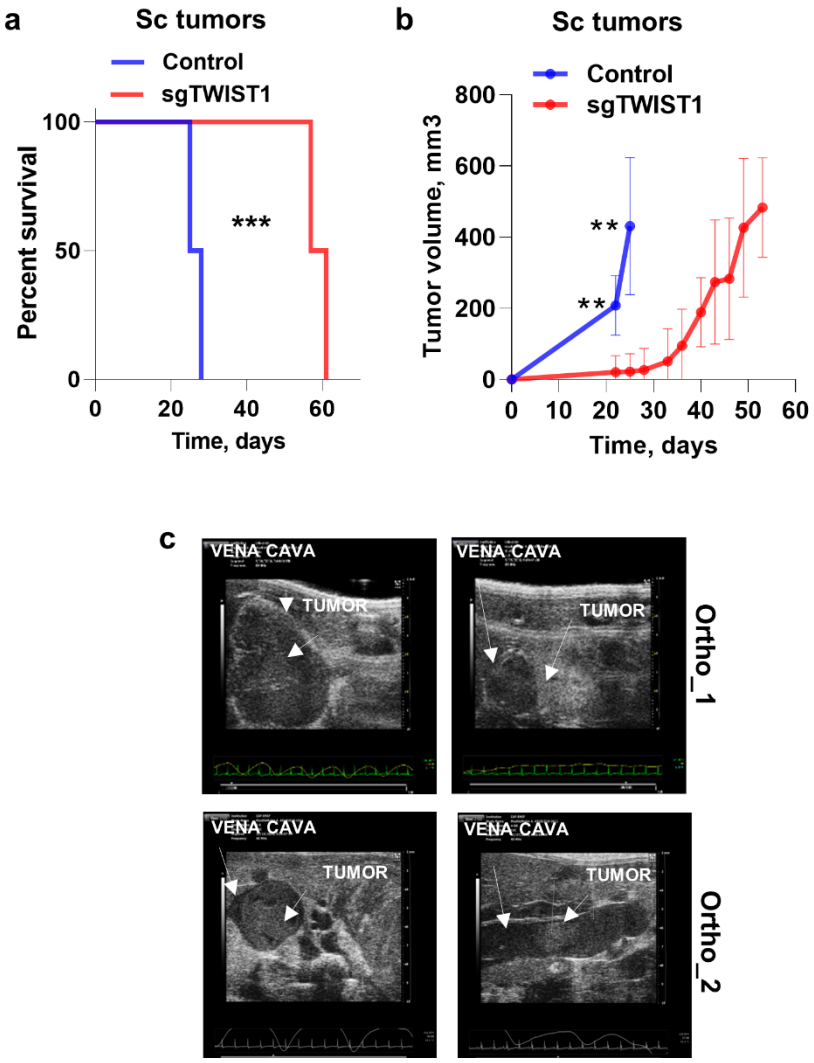

Supplementary Fig. 3. TWIST1 KO diminishes the tumor growth and invasive capacities of SK-N-Be2c cells. (**a**) Kaplan-Meier survival curve of mice implanted subcutaneously with SK-N-Be2c-Control or -sgTWIST1 cells. Mice were sacrificed once tumors reached approximately 700 mm^3. Tumor take: 100% (5/5) in both groups. Median survival in the Control vs sgTWIST1 groups: 26.5 vs 59 days. Gehan-Breslow-Wilcoxon test: ***p=0.0002. (**b**) Tumor growth curve for the sc experiment. Data are plotted as the mean tumor volume ± SD. Mann-Whitney t-test: **p= 0.0079 at both 22 and 25 days. (**c**) Representative ultrasound images of tumor cell intravasation in the vena cava of 2 distinct ortho_1 and ortho_2 Control mice.

Supplementary Figure 4

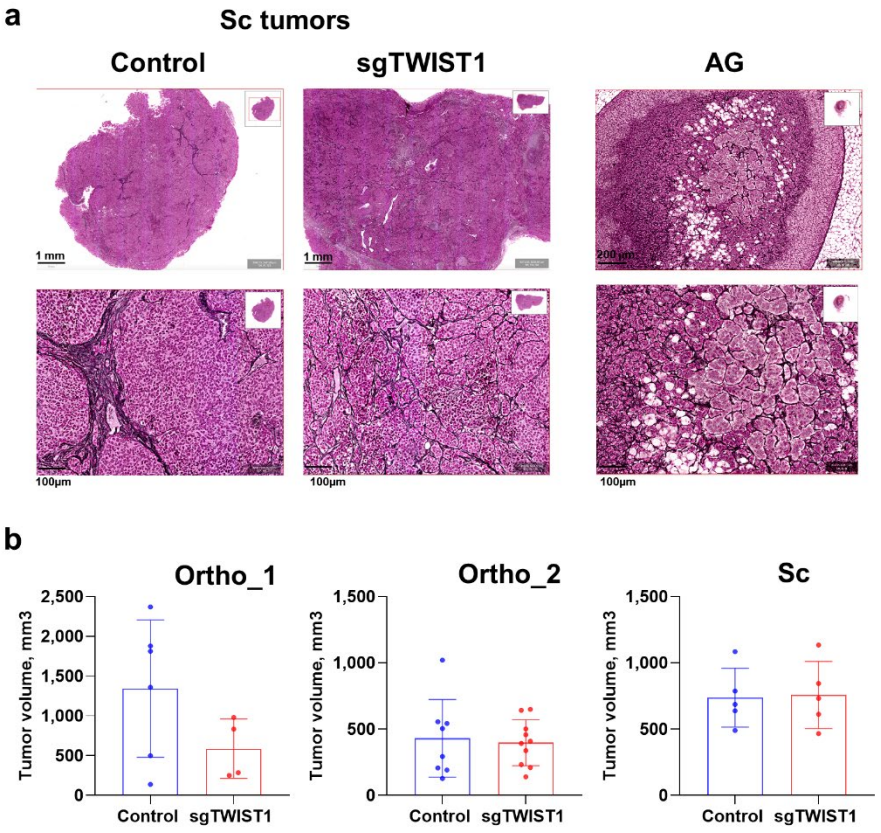

Supplementary Fig. 4. TWIST1 KO affects the the Collagen III/reticulin network organization. (**a**) Representative images of Gomori's staining showing the ECM architecture of Control and sgTWIST1 sc tumors (scale bars: top 1mm; bottom 100µm) as compared to the normal AG (scale bars: top 200 µm; bottom 100 µm). (**b**) Graphs illustrating the mean tumor volumes at sacrifice ± SD. Ortho_1: mean Control= 1343 mm^3, n=6; sgTWIST1= 587 mm^3, n=4; Mann-Whitney test: p= 0.257. Ortho_2*:* mean Control= 430 mm^3, n= 8; sgTWIST1= 397 mm^3, n=10; unpaired t-test: p= 0.. *SC*: mean Control: 737 mm^3, n=5; sgTWIST1= 757 mm^3, n=5; Mann-Whitney: p>0.999.

Supplementary Figure 5

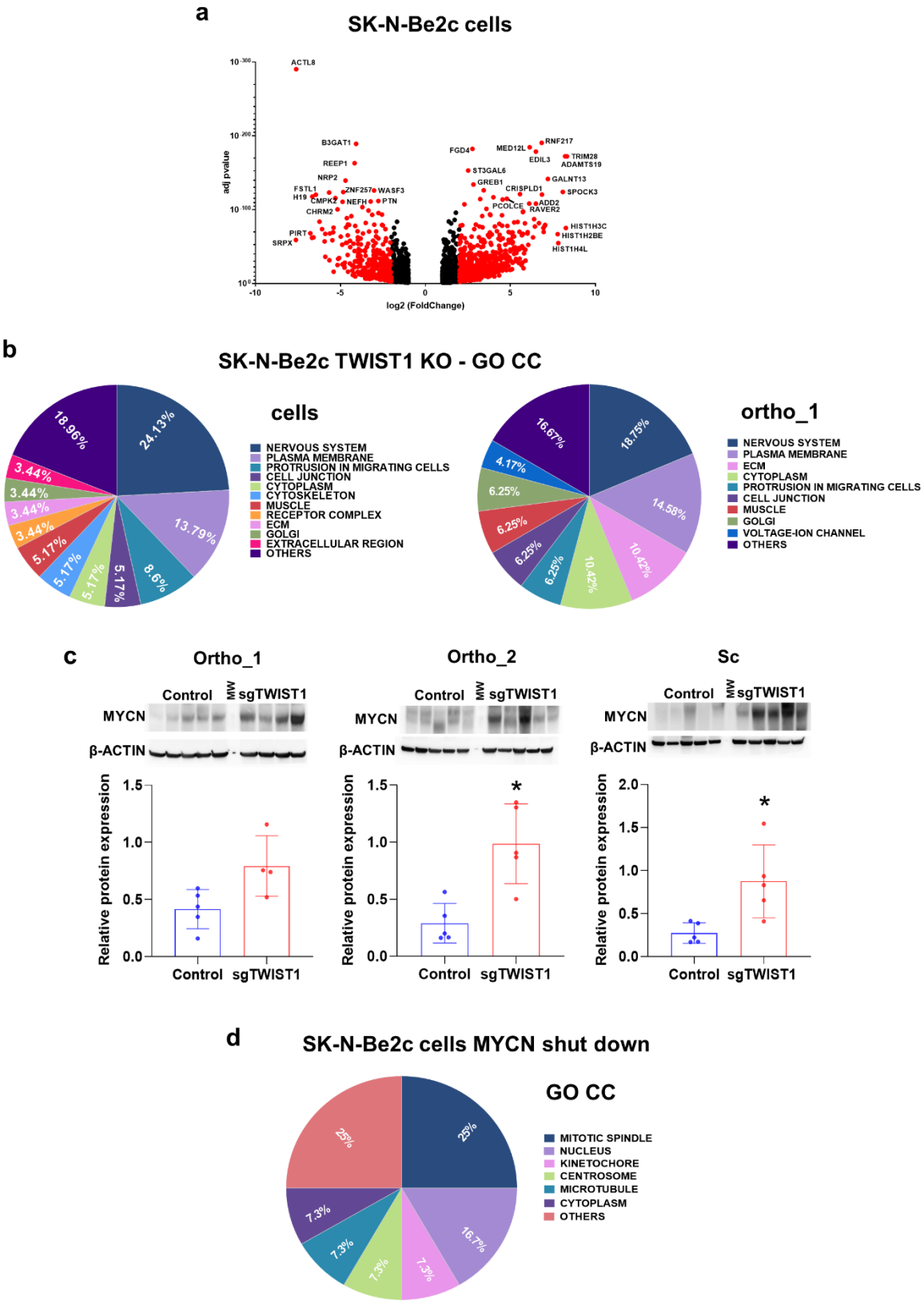

Supplementary Fig. 5. Distinct transcriptional programs are affected upon TWIST1 KO and MYCN shut down. (**a**) Volcano plots showing the distribution of the gene expression fold

changes and adjusted *p* value for the DE genes in SK-N-Be2c-Control versus SK-N-Be2c–sgTWIST1 cells. Genes with False Discovery Rate (FDR) < 0.05 and absolute value (av) of log2(FC) ≥ 1 were considered as DE; in red genes with av of log2(FC) ≥2, in black genes with av of log2(FC) ≥ 1 and <2. Positive and negative x-values represent genes either up or down-regulated by TWIST1 respectively. (**b**)**.** Illustration of the cellular components gene sets found enriched by GO analyses (GO CC) in the DE genes following TWIST1 KO for both SK-N-Be2c cells (left panel) and ortho_1 tumors (right panel). Data are reported as the repartition (in %) of the diverse pathways identified with a FDR < 0.01 (n=58 for cells, n=48 for tumors). (**c**) Immunoblotting for MYCN protein and β-actin as control (upper panel) and densitometric quantification of MYCN expression relative to β-ACTIN (lower panel) in SK-N-Be2c-derived tumors of the 3 *in vivo* experiments. Expressions relative to β-ACTIN were plotted as individual data with mean ± SD. Mann Whitney test. **p*= 0.0159 in ortho_2 and sc. Ortho_1: n= 5 Control; n= 4 sgTWIST1; ortho_2 and sc: n= 5 Control; n= 5 sgTWIST1. (**d**) Illustration of the GO CC gene sets found enriched in the DE genes of SK-N-Be2c cells upon JC1-medited MYCN shutdown. RNAseq data of SK-N-Be2c cells treated with JC1are during 24h or DMSO as control were uploaded (GSE80154, see Methods) (Zeid et al.). Genes with False Discovery Rate (FDR) < 0.05 and absolute value (av) of log2(FC) ≥ 1 were considered as DE. Data are reported as the repartition (in %) of the diverse pathways identified with a FDR < 0.01 (n=24).

Supplementary Figure 6

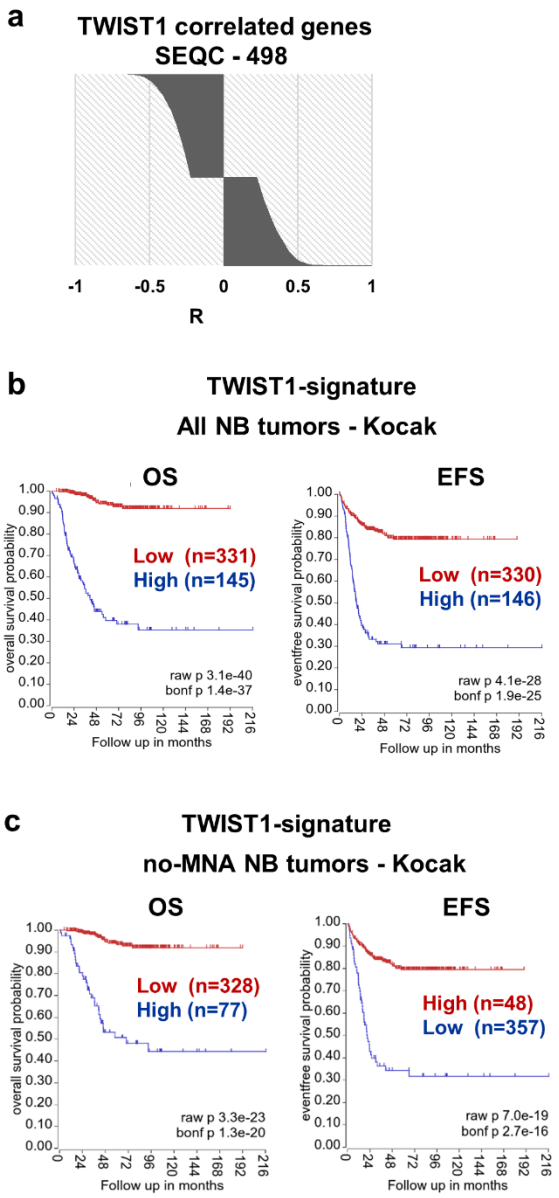

Supplementary Fig. 6. Identification of a TWIST1-signature associated with poor survival in NB. (**a**) Illustration of the 7737 genes correlated with TWIST1 expression in the SEQC dataset of NB primary tumors with the repartition of the R values. Source probeset: NM_000474; R *p* value cutoff: 0.01; Corr. multiple testing: Bonferroni. (**b-c**) Kaplan-Meier OS and EFS survival curves associated with the expression of the TWIST1-signature both in the complete Kocak cohort with survival data (n=476) (**b**) and in the no-MNA sub-cohort (n=405) (**c**). Expression cutoff: 0.03 for both curves.

Supplementary Figure 7

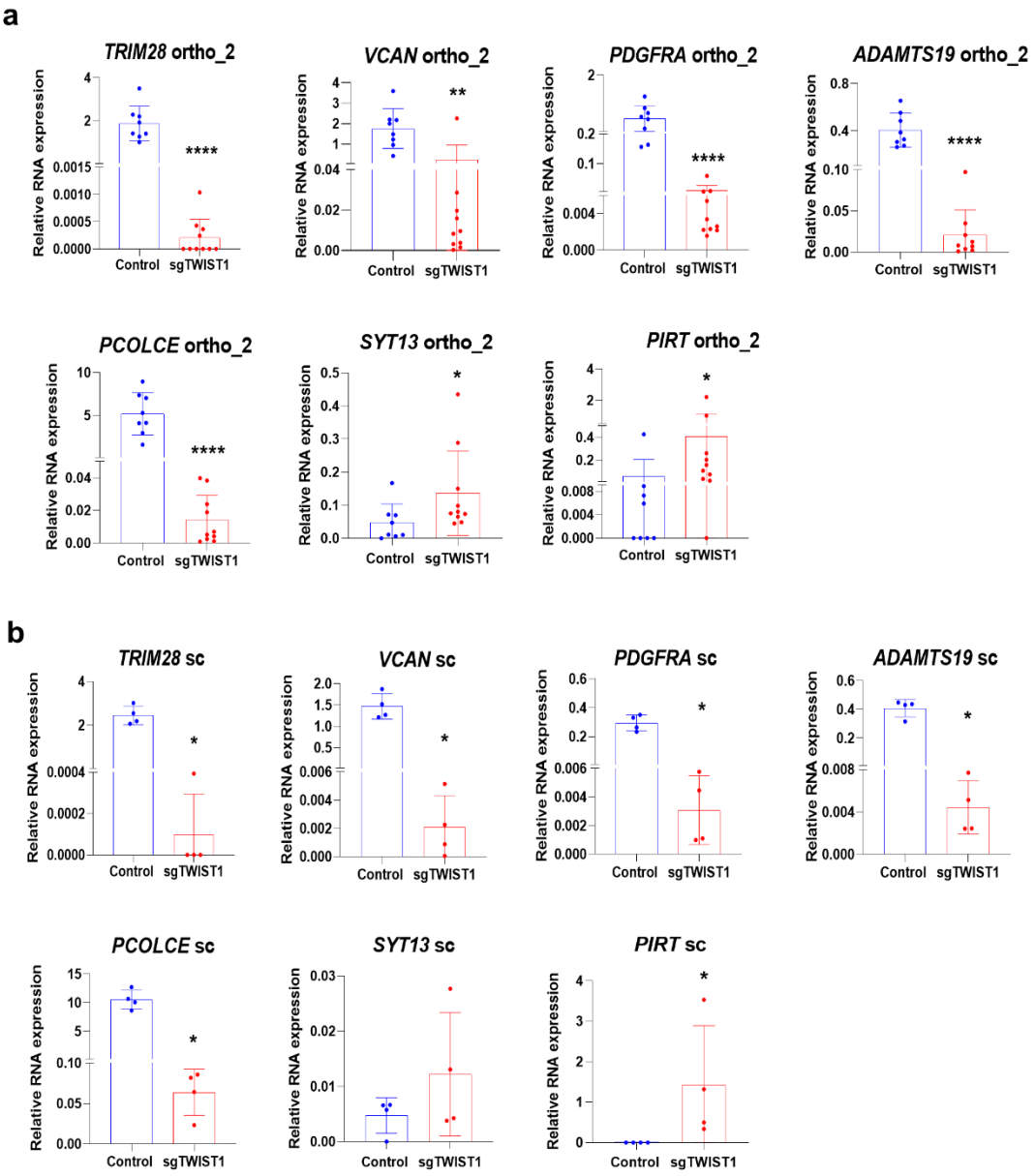

Validation of TWIST1-mediated deregulation of selected TWIST1 target genes at the RNA level in SK-N-Be2c-derived tumors. (**a-b**) mRNA expression levels of the selected TWIST1 target genes relative to *HPRT1* analyzed by RT-qPCR are plotted as individual values with mean ± SD for the indicated *in vivo* experiments**.** Numbers of tumors analyzed for ortho_2 (**a**): Control n= 8, sgTWIST1 n= 10; and for sc (**b**): Control n= 4, sgTWIST1 n= 4. Statistical analysis was performed using Mann Whitney test for all genes but *PCOLCE in* ortho_2 experiment (unpaired t-test: ****p<0.0001). Ortho_2: *TRIM28*: ****p=0.0001 2; *VCAN*: **p=0.0021; *PDGFRA* and *ADAMTS19*: ****p=0.0001; *PIRT*: *p=0.0146; *SYT13*: *p=0.0266; sc: *TRIM28*: *p=0.; *VCAN*, *PDGFRA*, *ADAMTS19* and *PIRT*: *p=0.0286; SYT13: *p=0.0266.

Supplementary Figure 8

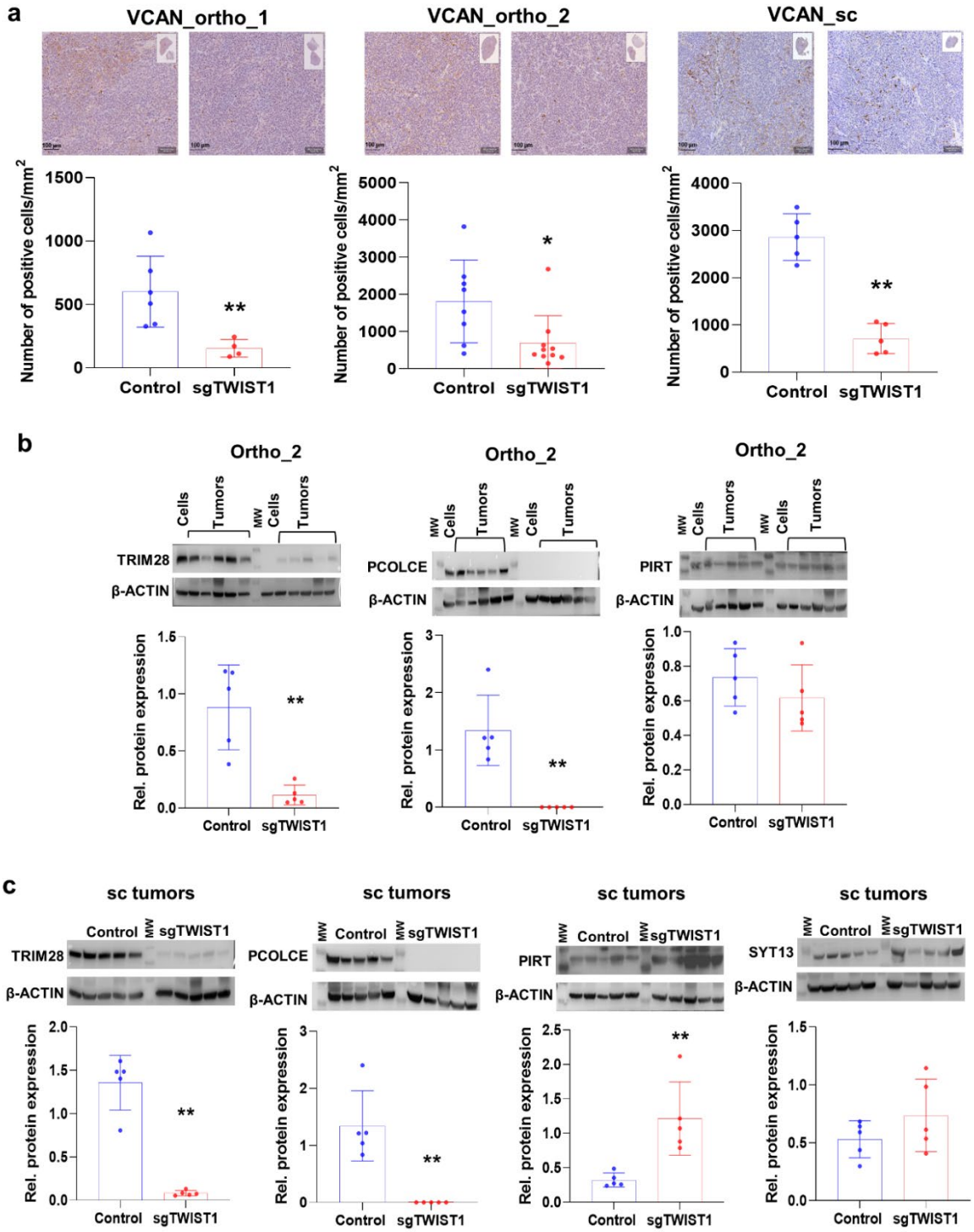

Supplementary Fig. 8. Analysis of the protein expression levels of selected TWIST1 target genes in SK-N-Be2c-derived tumors. (**a**) Upper panels: representative images of IHC for VCAN in the indicated tumors (scale bar =100 μm); lower panels: quantification of VCAN

staining (Qpath software on total area of each section). Mann-Whitney: ortho_1:**p=0.0095, n=6 Control and n=4 sgTWIST1; ortho_2: *p= 0.0155, n=8 Control and n=10 sgTWIST1; sc: **p=0.0079, n=5 Control and n=5 sgTWIST1. (**b-c**). Relative protein expression as determined by immunoblotting for the selected genes in the ortho_2 (**b**) and the sc (**c**) tumors. Upper panel: Representative images of immunoblotting for TRIM28, PCOLCE, PIRT and SYT13 (β-ACTIN as the control); MW: molecular weight; lower panel: densitometric quantifications of immunoreactive band densities. Expressions relative to β-ACTIN were plotted as individual data with mean ± SD. Mann Whitney test: **p=0.0079 for all comparisons. Ortho_2 and sc: n=5 Control and n=5 sgTWIST1.

Supplementary Figure 9

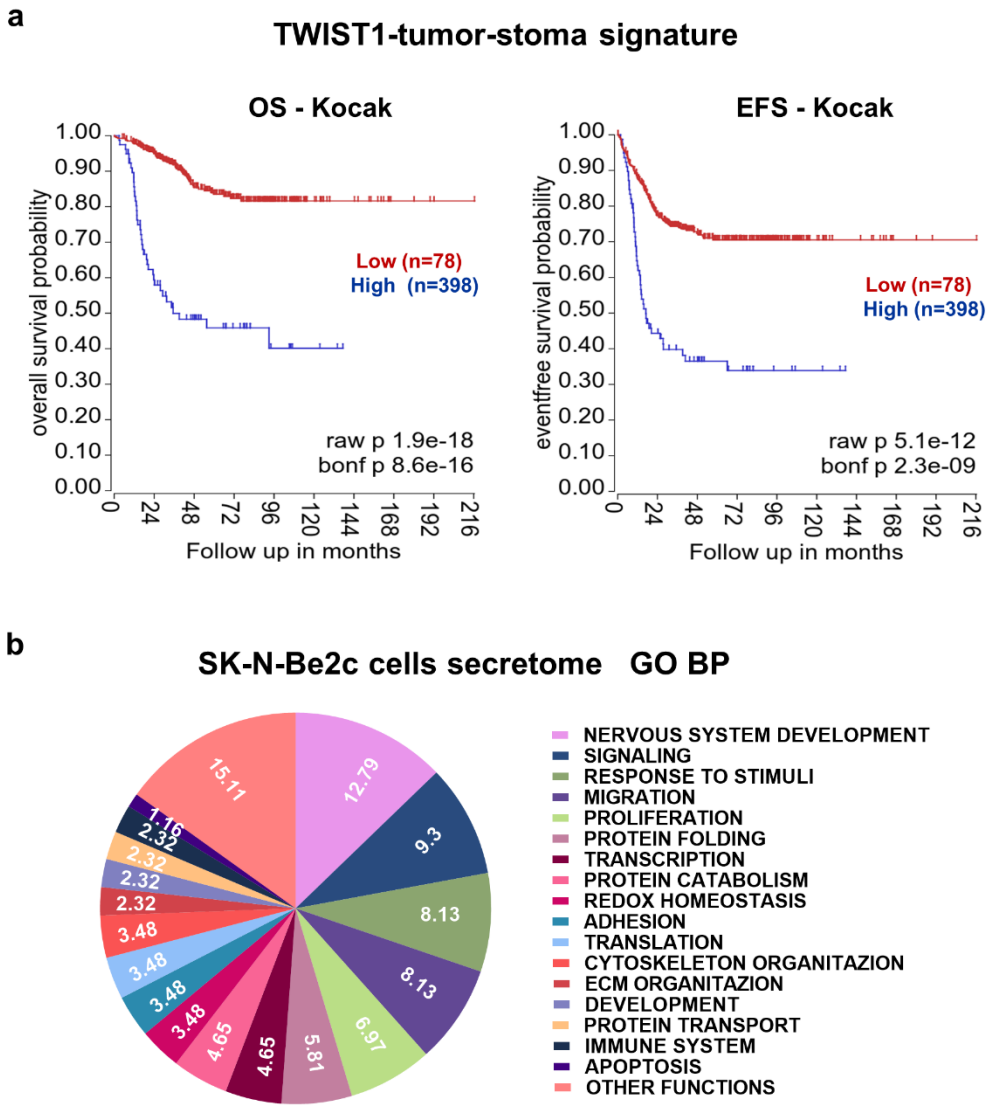

Supplementary Fig. 9. **Correlation between the TWIST1-tumor-stroma signature in the Kocak NB dataset and the outcome of patients.** (**a**) Kaplan-Meier plots showing the correlation between a high level of the paracrine signature expression and a poor OS and EFS of NB patients in the Kocak dataset. Expression cutoff for both curves: 0.14. (**b**) Illustration of biological processes (BP) found enriched by gene ontology analysis for the DE proteins in SK-N-Be2c cell secretome. Data are reported as the repartition (in %) of the diverse BP identified with a FDR < 0.01 (n=50).

Supplementary Figure 10

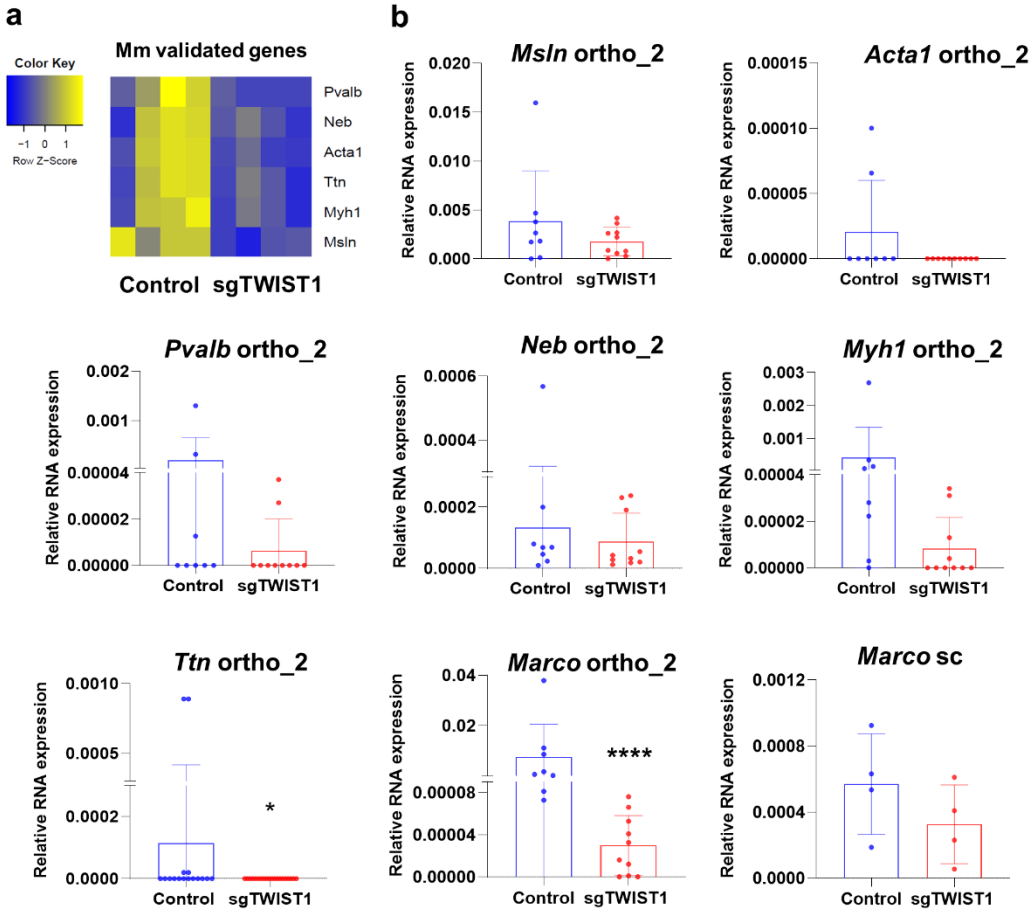

Supplementary Fig. 10. **Validation of selected genes of the myofibroblast signature in the ortho_2 and sc tumors by real-time PCR.** (**a**) Heatmap showing the RNA expression levels (z-score) of the Myofibroblasts signature selected genes as determined by RNAseq analysis in ortho_1 tumors. (**b**) mRNA expression levels for the selected myofibroblast genes and *Marco* relative to *β-actin* as determined by RT-qPCR. Data are plotted as individual values with mean ± SD. Mann Whitney test: Ortho_2: *Ttn*: **p*= 0.0309; *Marco*: *****p*<0.0001. Ortho_2 tumors: Control n=8; sgTWIST1 n=10; sc tumors: Control n=4, sgTWIST1 n=4.